Proton Gyro-harmonic Echoes Observed by the RPI Instrument on the IMAGE Satellite

D. L. Carpenter,[1] T. F. Bell,[1] D. Chen,[1] D. Ng,[1] C. Baran,[1] B. W. Reinisch,[2] I. Galkin[2]

Abstract.

At altitudes ranging from $\approx$ 1500 km to 20,000 km in the plasmasphere, 3.2-ms pulses from the Radio Plasma Imager (RPI) instrument on the IMAGE satellite (scanning the frequencies from 6 to 63 kHz or 20 to 326 kHz) can couple strongly to protons in the immediate vicinity of the satellite. The result is a variety of echo forms, several of which carry signatures of, or arrive at, multiples of the local proton gyroperiod t_p. Lower-altitude ($<$ 4,000 -km) versions of two of these proton gyroharmonic (PGH) forms were observed in the topside ionosphere by sounders in the ISIS satellite era, namely discrete echoes above the electron gyrofrequency f_{ce} and spur-like broadenings of resonances such as the one at the electron plasma frequency f_{pe}. On IMAGE the occurrence rates of PGH echoes above f_{ce} were highest when the average angle ϕ between the spacecraft velocity vector $\mathbf{V_S}$ and the geomagnetic field $\mathbf{B}$ at $\approx$ 12,000 km was small, near 20°, but on occasion such echoes were detected when ϕ approached 90°. A new PGH echo form, apparently confined to altitudes above $\approx$ 7,000 km, is a resonance centered at a frequency $\approx$ 15% above f_{ce}. Also new are exceptionally strong echoes in the whistler-mode domain near 10 kHz, called WM echoes. These were observed at all altitudes below $\approx$ 9,000 km. When the angle ϕ was near a local minimum of order 10°, WM echoes were observed to repeat at multiples of t_p up to 15 or more. The data indicate that echo detection near 10 kHz was largely confined to a region of radius $\approx$ 300 m around the field line of excitation, and that the peak excitation of the protons occurred as a transient event at the beginning of each rf pulse. We found evidence of at least three different PGH mechanisms. In the case of WM echoes there is spatial bunching of accelerated protons during formation of an electron sheath around the positive-voltage antenna element. The gyrating protons then produce a series of quasi-electrostatic pulses at multiples of t_p following the leading edge of the transmitter pulse. The most efficient proton excitation is expected to occur at frequencies near and below the proton plasma frequency f_{pp}, which is consistent with observed variations in WM echo activity with altitude and pulse frequency. In contrast to WM echoes, the discrete PGH echoes above f_{ce} and near f_Z show evidence of thermal-mode wave propagation at the rf frequency of the sounder pulses, while the resonance above f_{ce} suggests the existence of a ringing phenomenon in the plasma that is unique to altitudes above $\approx$ 7,000 km. Previously suggested processes that we consider relevant to PGH echo phenomena above f_{ce} include: (i) coupling between an excited Z-mode wave and longitudinal plasma waves [*Benson*, 1975], (ii) the accumulation of negative charge on an electric antenna during an rf pulse [*Oya*, 1978], and (iii) Bernstein-mode propagation to an antenna from an excited proton population [*Muldrew*, 1998].

1. Introduction

1.1. Sounder-stimulated Proton Gyroharmonic Echo Phenomena

It is well known that data records of radio sounders operating in space include not only echo traces associated with propagation along ray paths extending to distant reflection points [e.g., *Hagg et al.*, 1969; *Reinisch*

[1]Space, Telecommunications and Radioscience Laboratory, Stanford University, Stanford, California, USA.
[2]Center for Atmospheric Research, University of Massachusetts, Lowell, Massachusetts, USA.

et al., 2001], but also evidence of interactions between sounder pulses and plasmas in the immediate vicinity of the spacecraft [e.g., *Calvert and McAfee*, 1969; *Benson*, 1977]. These local interactions represent a challenge to understanding the behavior of electric antennas in space plasmas and to the planning of future wave injection missions.

One local reaction to sounder pulses, of special interest in this paper, involves echoes whose arrival times correspond closely to the proton gyro-period t_p at the location of the satellite. On the ionograms of the ISIS-series sounders, operating at altitudes less than 4000 km, such proton gyroharmonic (PGH) phenomena appeared in two principal forms: (1) discrete echoes at frequencies just above the electron gyrofrequency f_{ce}, with delays close to t_p [e.g., *Horita*, 1987; *Oya*, 1978], and (2) spurs, variously shaped broadenings along resonance spikes located at the plasma frequency f_{pe} or at multiples of f_{ce}, and occasionally at the upper hybrid frequency f_{uh} [e.g., *King and Preece*, 1967; *Benson*, 1975; *Horita*, 1987]. The time delays to the spurs were consistent with the proton gyroperiod and multiples thereof. Various physical mechanisms for these effects have been proposed, including a process [*Muldrew*, 1998] by which protons passing near an antenna retain memory of a pulse and return that pulse to the satellite as an 'echo' one gyroperiod later.

As might be expected, PGH echoes appear in the records of the Radio Plasma Imager (RPI) on the IMAGE satellite [e.g., *Reinisch et al.*, 2001], the first high powered sounder to operate close to and also well above the altitudes of the Alouette/ISIS series. IMAGE was launched in March, 2000 into a polar orbit with apogee nominally at $\approx 8\ R_E$ geocentric distance and perigee at $\approx 1{,}200$ km altitude [e.g., *Burch*, 2000; 2001]. RPI not only stimulates versions of PGH echo forms previously detected at ionospheric heights, but also produces novel phenomena such as: (1) strong echoes near 10 kHz in the whistler-mode domain, usually followed at multiples of t_p by additional echoes, and (2) a resonance centered at a frequency $\approx 15\%$ above f_{ce}.

The richness of the PGH echo forms reported here follows in part from the fact that RPI was able to operate in parts of the plasmasphere where f_{ce} is as low as $\approx$ 10 kHz. In contrast, the ISIS-series sounders [*Franklin and Maclean*, 1969] were restricted to regions where f_{ce} exceeds ≈ 200 kHz. The topside sounders were not designed to record whistler-mode-domain signals below $\approx$ 100 kHz, while the low-frequency limit of RPI sounding was regularly in the range 5 to 20 kHz. ISIS sounder pulse lengths were of order 100 μs, thus providing time-delay resolution a factor of ≈ 30 better than that available to RPI with its 3.2-ms minimum pulse length [*Reinisch et al.*, 2000]. However, by recording echo travel times that regularly extended to ≈ 180 ms and occasionally to $\approx$ 300 ms, RPI could observe echo delays (including high-order multiples of short initial delays) a factor of up to 30 times longer than those available to (or expected by) ISIS. On the ISIS satellites, the effective bandwidth for detection was typically ≈ 60 kHz, which was satisfactory for observing echoes extending over hundreds of kilohertz in frequency at nearly constant time delay. In the case of RPI, the nominal 3-dB bandwidth was ≈ 300 Hz, which was ideal for operations below 100 kHz and for the identification of echoes or resonances that are confined to frequency bands only several kHz wide. This paper offers an initial description of PGH echoes detected by RPI and a brief discussion of some of the factors that may influence PGH echo generation.

RPI is a multi-mode instrument [*Reinisch et al.*, 2000]

in which sounding and listening frequencies, range detection, pulse characteristics and repetition rate are adjustable parameters over a wide range of values. The instrument covers the frequency range from 3 kHz to 3 MHz with a receiver bandwidth of 300 Hz. Originally there were three orthogonal thin-wire antennas, two 500-m tip-to-tip dipoles in the spin plane (X and Y) and a 20-m tip-to-tip dipole along the spin axis (Z). The long dipoles were used for transmission, and all three antennas were used for reception. The nominal radiated power from RPI, varying (in terms of free-space-mode excitation) from 0.1 mW at low frequencies to $\approx$ 10 W per dipole at 200 kHz and above, was reduced by 3 dB on May 8, 2000 when the power supply for the Y-axis transmitter failed. A further reduction occurred on October 3, 2000, when one of the X-axis monopoles was partially severed, apparently by a micrometeorite. On September 18, 2001 an unknown (presumably small and negligible) section of the Y antenna was lost, and beginning on September 30, 2004, the sensitivity of the Y-antenna data was substantially reduced by damage to the +Y element. In spite of these difficulties, the X antenna continued to perform well as a transmitting and receiving element, as did the Z antenna as a receiving element. Unless otherwise indicated, our report is based upon data from the X antenna. IMAGE data acquisition was interrupted on December 18, 2005, due to an apparent failure in the power distribution unit.

1.2. Time-Delay-Versus-Frequency Forms of PGH Echoes

The PGH phenomena reported here have been observed primarily within the plasmasphere or the plasmasphere boundary layer (PBL) at altitudes ranging from near perigee at $\approx$ 1,500 km to $\approx$ 20,000 km. Most of the events appear as responses to single 3.2-ms sounder pulses at frequencies that are stepped upward from a starting value in the whistler-mode domain. Figure 1 is a dispersion diagram for propagation in a cold plasma. The axes have been interchanged so as to display wave number k versus frequency f in a manner similar to that in which time delay (or range) is displayed versus frequency on RPI 'plasmagrams.' The illustrated relations among wave-propagation domains are representative of those extensive portions of the plasmasphere within which the ratio of plasma frequency to gyrofrequency f_{pe}/f_{ce} exceeds unity (for the case illustrated, $f_{pe}/f_{ce} = 2$ was used). A horizontal arrow indicates the range of frequencies of primary interest in our study.

The whistler-mode domain, with upper limit at the electron gyrofrequency f_{ce}, is followed at higher frequencies by a band of no propagation that extends to:

$$f_Z = (f_{ce}/2)[-1 + (1 + 4(f_{pe}/f_{ce})^2)^{1/2}], \qquad (1)$$

the lower limit of the left-hand polarized, supra-luminous, branch of the Z mode (corresponding to region 4 on a CMA diagram). This stop-band exists when the ratio of electron plasma frequency to electron gyrofrequency f_{pe}/f_{ce} exceeds $\sqrt{2}$.

The various PGH echo forms are illustrated in Figures 2, 3, and 4 on RPI records that display echo delay in ms (for the X antenna) versus sounder frequency in kHz, color coded according to intensity in dBnV/m. The forms illustrated are: (1) f_{ce}^+ echoes, discrete forms that appear at frequencies $\approx$ 10-25% above f_{ce}; (2) f_{ce}^+ resonances, spike-like features that appear at frequencies $\approx$ 15% above f_{ce}; (3) WM echoes, discrete forms that appear in the whistler-mode domain below $\approx$ 50 kHz; (4) Z echoes, discrete forms that usually appear at frequencies

above ≈ 200 kHz within and near the Z-mode propagation domain.

Figure 2 shows an $f_{ce}{}^+$ echo on a record of time delay from ≈ 40 to 100 ms versus frequency from 20 to 50 kHz. IMAGE was at L ≈ 3.7, well inside an extended plasmasphere at an altitude of $\approx 14{,}000$ km and in the mid-afternoon sector. The local electron density was $\approx 560\ el - cm^{-3}$. The sounding format involved single 3.2-ms pulses transmitted at 250-ms intervals as frequency was increased in steps of 300 Hz from 6 kHz to 63 kHz (single pulses at each frequency were used in all the cases reported here).

On Figure 2 the local value of f_{ce} is well defined at ≈ 30.3 kHz by a resonance spike, a type of response that is regularly present on sounder records from the topside ionosphere [e.g., *Benson*, 1977 and references cited therein]. A band of whistler-mode noise extends upward in frequency to a relatively sharp cutoff at ≈ 26 kHz. This band is attributed to multi-path propagation and scattering of a variety of whistler-mode signals, including naturally occurring wave emissions, whistler-mode emissions triggered by lightning, and multiple whistler-mode signals from ground-based transmitters. The quiet band just below f_{ce} is essentially an effect of accessibility, a narrow band of whistler-mode frequencies within which bending of rays from distant sources becomes locally strong. The effect is similar in nature to that of an exterior caustic surface, as illustrated in satellite observations of ground transmitters by *Sonwalkar et al.* [1994].

In Figure 2, the $f_{ce}{}^+$ echo first appears at ≈ 33.3 kHz, ≈ 3 kHz above f_{ce} in frequency, and extends to 39 kHz. It exhibits a time-delay-versus-frequency form something like that of a hockey stick, at first falling steeply in delay with increasing frequency and then curving to reach a constant delay of ≈ 61 ms. As indicated below, that delay corresponds closely to the local proton gyro-period $t_p = 1836/f_{ce}$.

The plasmagram in Figure 3 represents a similar program, but in this case the entire plasmagram is displayed, time delay from 0 to 178 ms versus frequency from 6 to 63 kHz. Wave activity at the RPI antennas was sampled at intervals of 3.2 ms, but the measurements at t = 3.2 ms, 6.4 ms, and 9.6 ms were not displayed so as to account for the 3.2-ms-long transmitter pulse and to allow additional time for the receiver to recover from the high voltage generated during the pulse. After February 2005, only the first data bin was omitted, and plasmagram displays of measured activity began at t = 6.4 ms instead of 12.8 ms.

At the time of Figure 3, IMAGE was at L ≈ 3.6 and at an altitude of $\approx 12{,}000$ km, again well inside the plasmasphere. There are three PGH effects, a WM echo, $f_{ce}{}^+$ echoes, and an $f_{ce}{}^+$ resonance. The WM echo, extending from ≈ 9 to 17 kHz at a constant delay of ≈ 45 ms, appears as a discrete intensity enhancement within the usual whistler-mode noise background. The value of f_{ce} is well marked by a tapered resonance spike at ≈ 42 kHz. Approximately 3 kHz above $f_{ce}{}^+$ is an '$f_{ce}{}^+$ resonance,' a new phenomenon that does not appear to have a counterpart in topside sounder data. The resonance differs from the spike at f_{ce} in that it extends to the top of the record and (in this case) is not clearly defined in the first ≈ 30 ms after the beginning of the transmitter pulse. Along the high-frequency side of the $f_{ce}{}^+$ resonance are $f_{ce}{}^+$ echoes that arrived at equal intervals, the first at ≈ 44.5 ms, the second at ≈ 89 ms, and the third at ≈ 133 ms.

There are differences in amplitude among the PGH effects in Figure 3: portions of the WM echo near 10 kHz are ≈ 10-15 dB stronger than the $f_{ce}{}^+$ resonance or

f_{ce}^+ echoes.

The plasmagram of Figure 4 is from a sounding program in which single 3.2-ms pulses were transmitted as frequency was stepped in 1200-Hz increments from 20 kHz to 326 kHz. This entire range is displayed, but the time scale is here limited to 0 to $\approx$ 85 ms. IMAGE was at L $\approx$ 2.9 and at an altitude of $\approx$ 11,500 km, well inside an extended afternoon plasmasphere. A weak f_{ce} resonance spike appears at $\approx$ 78 kHz, while $2f_{ce}$ and $3f_{ce}$ resonances are clearly defined. These differences in intensity and duration are similar to relations found among nf_{ce} resonances in topside sounder data [e.g., *Benson,* 1977].

Figure 4 provides a view of PGH effects occurring essentially simultaneously within three of the frequency domains indicated by the horizontal arrow in Figure 1. Between 20 and $\approx$ 35 kHz, at a delay of $\approx$ 23 ms, are portions of a WM echo. An f_{ce}^+ echo appears at $\approx$ 85 kHz, with a lowest delay that is also $\approx$ 23 ms. A second f_{ce}^+ echo appears at delays that are twice those of the first. Then at the far right is a discrete Z echo that extends from 280 kHz to the upper frequency limit of the record, again at a delay of $\approx$ 23 ms (within the uncertainty imposed by the 3.2-ms interval between range bins). Further examination of this and other records showed that the value of f_Z was $\approx$ 304 kHz. Thus we conclude that the discrete Z echo extended in frequency from a point well inside the non-propagating band into the L-X propagation domain.

The WM echoes were again stronger than the f_{ce}^+ echoes (here by $\approx$ 20 dB). The Z echoes increased in intensity with frequency, such that near 315 kHz within the L-X domain they saturated the receiver.

1.3. Previous Suggestions About PGH Echo Mechanisms

Each of the several phenomena described above appears to originate in a particular proton 'memory' process excited in the vicinity of the IMAGE satellite. However, it is not clear what various physical processes are required to store the rf pulse information and then couple it back from the proton distribution to the satellite. A number of efforts have been made to explain PGH effects observed on the ISIS series satellites, prominent examples being those of *Benson,* [1975], *Oya,* [1978], and *Muldrew,* [1998].

Benson [1975] focused attention on PGH spurs detected on ISIS-series resonance spikes, suggesting that those that were most intense and widely extended in time delay and frequency were the result of strong coupling of sounder pulses to the plasma at resonances such as the one at f_{pe} when it overlaps a multiple of f_{ce}. When f_Z is close to but below nf_{ce}, extra energy can be fed into longitudinal plasma waves associated with the nf_{ce} resonances due to wave mode coupling between an excited Z-mode wave and the longitudinal plasma waves. This coupling is possible because the dispersion curves for the two waves directly connect under these conditions. An anisotropy of the electron velocity distribution, such that $t_\perp > t_\parallel$, is stimulated by the cyclotron damping of the plasma waves. The resulting instability, called the Harris instability, can then give rise to excited ion motions that couple to the electron motions associated with the resonance.

Oya [1978] focused upon discrete PGH echoes just above f_{ce}, such as those detected on Alouette 2. As summarized by *Muldrew* [1998], Oya proposed a multi-element process in which protons in the plasma sheath are bunched by a sounder pulse and given a specific velocity parallel to the magnetic field **B** that depends upon the

spacecraft velocity $\mathbf{V_S}$. The protons come together one or more cyclotron periods later to produce a pseudo-wave. As a result of the pulse, the sounder excites electrostatic electron cyclotron harmonic waves. These waves are Landau damped, giving rise to an energetic electron stream. The interaction of this stream with the pseudo-waves created by the protons leads to a wave that propagates to, and can be detected by, the sounder.

Muldrew [1998], in discussing the discrete PGH echoes just above f_{ce} observed on the ISIS series, proposed that they occur as a result of a memory process involving the protons passing near the satellite antenna. The protons are perturbed in such a way that one gyro-period later they can coherently replicate the rf pulse that has been imposed. An electron Bernstein-mode wave is generated in the heated plasma, propagating in a direction orthogonal to the magnetic field lines along which the perturbed protons are distributed. The wave will then reach the satellite antenna with an overall delay that combines the proton gyroperiod with the additional group delay associated with Bernstein wave propagation.

On the ISIS sattelites, the time delays of discrete PGH echoes could be measured to an accuracy of a fraction of a millisecond. Because of this and the availability of constant as well as swept-frequency sounding, it was possible in one case for *Muldrew* [1998] to study small, few-percent temporal variations in the echo delays and to interpret these as evidence of a propagation delay from a source region of excited protons to a moving antenna. Since Bernstein wave velocity is electron temperature dependent, Muldrew was able to use the observed delay information as a diagnostic of local electron temperature. He further found that by using the calculations of Bernstein wave group velocity of *Tataronis and Crawford*, [1966], he could explain an observed increase in Bernstein wave group delay with decreasing frequency as f_{ce} is approached from above. That additional delay was noted in the ISIS series data [e.g., *Horita*, 1987], but was detectable only at the level of a few percent, while on RPI, as illustrated in Figure 2, the effect can be 20% or more.

The following sections describe various properties of $f_{ce}{}^+$ echoes, $f_{ce}{}^+$ resonances, WM echoes, and Z echoes. In a later section we comment on PGH mechanisms, emphasizing WM echoes near 10 kHz and the role of the antenna sheath.

2. PGH Echo Properties

2.1. Properties of the $f_{ce}{}^+$ Echoes

In the months of May, June, and July 2004 an $f_{ce}{}^+$ echo was detected at least once on 103 of 169 IMAGE orbits. The sounding program in use was limited to frequencies above 20 kHz and frequency steps of 1200 Hz (as in Figure 4). Fortunately, a program with 300-Hz frequency resolution and coverage of the range 6 to 63 kHz was operated at plasmasphere altitudes during an $\approx$ 8-day period in August, 2004. In that period, $f_{ce}{}^+$ echoes were recognizable on 50 of the 114 individual soundings that stepped through the local value of f_{ce}. Figure 5 shows meridional locations along IMAGE orbits where the more clearly defined of these echoes were received. In each case IMAGE was inbound, passing through the near-equatorial plasmasphere and downward through the northern plasmasphere lobe.

Although, as noted, $f_{ce}{}^+$ echoes tended to be weak in comparison to events in the whistler-mode domain, their recognition was facilitated by the fact that the background noise level in the no-propagation band above f_{ce}

(see Figure 1) was usually 20-30 dB below typical noise levels in the whistler-mode domain. The ratio f_{pe}/f_{ce} was typically >2, so that the quiet band extended more than 100 kHz above f_{ce}.

To illustrate the tracking of the echoes with f_{ce}, Figures 6a through 6e show five successive plasmagrams from the afternoon plasmasphere as altitude decreased from $\approx$ 18,900 km to $\approx$ 12,900 km. The locations of the five soundings are marked by filled circles in Figure 5. The full 0-to-178 ms time-delay range of each plasmagram is shown.

In Figure 6a f_{ce} is 13.5 kHz and a steeply downward slanting echo with delay between $\approx$ 145 ms and 165 ms appears in a narrow frequency range at $\approx$ 16 kHz. Then in Figure 6b f_{ce} appears at $\approx$ 16.5 kHz and the f_{ce}^+ echo has shifted accordingly to a narrow frequency range around 19.5 kHz. As further illustrated in Figures 6c, 6d, and 6e, f_{ce}^+ echoes at frequencies roughly 15% above f_{ce} continued to appear as f_{ce} increased, reaching 42.3 kHz in the case of Figure 6e (Figure 6d is a complete version of the plasmagram of Figure 2).

Examples of f_{ce}^+ resonance effects appear sporadically in Figure 6, being weakly defined in Figures 6b and 6e and well defined in Figure 6c, where the f_{ce}^+ echoes appear on the high-frequency side of the resonance spike.

The tracking of f_{ce}^+ echoes with f_{ce} is demonstrated in Figure 7 by a plot of the ratio of the f_{ce}^+ echo frequency to f_{ce} for the more clearly defined events from the August 14-August 22, 2004 period of interest. The measurements of the f_{ce}^+ echo frequency were made at the mid-frequency of the echo. The ratio remained between $\approx$ 1.1 and 1.25 over much of the f_{ce}^+ range.

Figures 6a-6e illustrate additional features of f_{ce}^+ echoes, namely higher-order echoes that arrive at integral multiples of the first echo delays. A 2d echo is visible in Figures 6c, 6d and 6e, while a 3d echo appears in Figure 6e. Such echo multiples were reported from ISIS-series data by, for example, *Oya* [1978] and *Horita* [1987].

As could be expected from the ISIS-series work, f_{ce}^+ delays were found to be closely related to the proton gyrofrequency f_{cp} at the position of the satellite, where f_{cp} = $f_{ce}/1836$. Figure 8 shows such a relation for the August 14-22, 2004 data, displaying t_{min}, the shortest detectable delay in a given f_{ce}^+ echo, versus f_{cp}. The solid curve represents the simple inverse relation between t_p and f_{cp}. It is clear that t_{min} follows closely the variation of t_p with satellite position.

2.1.1. Amplitude decrements between 1st, 2d and 3d-hop f_{ce}^+ Echoes

In six cases of f_{ce}^+ echoes we measured the change in amplitude from the echo at delay t_p to the one at $2t_p$, and in two cases the additional decrement to the echo at $3t_p$. The decrement from the 1st-hop echo to the 2d-hop ranged from $\approx$ 3 dB to 12 dB, being 3.2 dB in the case of Figure 3 and 5.1 dB, 5.8 dB, and 7 dB in Figures 6c, 6d, and 6e, respectively. The decrements from the 2d-hop to the 3d-hop echo were roughly the same as from the 1st hop to the 2d, namely 3.5 dB in the case of Figure 3 and 9.8 dB in the case of Figure 6e.

2.1.2. Variations in the Forms of the f_{ce}^+ Echo

Notable variations exist in the time-versus-frequency forms of the f_{ce}^+ echo. Most such echoes observed with 1200- or 300-Hz frequency resolution in 2004 exhibited the curvature toward longer delays near f_{ce} illustrated by the examples of Figures 2 and 6. However, an exception was found, illustrated in Figure 9a, in which echoes at roughly constant delay appear just above an f_{ce} spike at 24 kHz and also just below it in the whistler-mode domain.

A similar variety of forms was reported from ISIS-series work by *Horita* [1987], who found that while most discrete echoes were confined to a range of frequencies above f_{ce} and often exhibited curvature toward longer delays near f_{ce}, some remained at constant delay as they appeared both above and below the broad ($\approx$ 50-kHz-wide) f_{ce} spike. A similar event was reported by *Muldrew* [1998], in which a discrete echo at $\approx t_p$ appeared both above and below a 330-kHz gyroresonance spike and was particularly well defined during a fixed-frequency measurement at 250 kHz in the whistler-mode domain.

In 2005 a renewed effort was made with RPI to sound with 300-Hz frequency resolution in the 6-63 kHz range. When $f_{ce}{}^+$ echoes were observed, they exhibited forms generally similar to those found in the 2004 eight-day period. However, in many cases only the constant-time-delay (hockey-stick blade) part of the echo appeared, beginning above f_{ce} (often well above f_{ce}) and extending to values of f/f_{ce} larger than were typical of the 2004 data. Figure 9b shows an example from November 11, 2005 in which f_{ce} was 24.3 kHz, close to the value in Figure 9a, but the echo was confined to a range above $\approx$ 32 kHz, at values of f/f_{ce} between 1.36 and 1.44.

2.1.3. The 'Offset' of an $f_{ce}{}^+$ Echo From f_{ce}

When an $f_{ce}{}^+$ echo exhibited curvature, as in Figures 2 and 6, it appeared to approach a frequency of asymptotically long time delay that was offset from $f_{ce}{}^+$. The 'offset' may be estimated as the frequency difference between f_{ce} and an asymptotic lower frequency bound f_o found from fitting a curve of form

$$t_i = A/(f_i - f_o)^n + C, \qquad (2)$$

to the data points, where t_i is time delay or range at frequency f_i, and f_o, A, and n are parameters to be evaluated, and C is an asymptotic lower bound to the delay which can be estimated as t_p. In the event of Figure 2 and 6d, f_o was found to be 31.7 kHz. Curve fitting was applied to nine of the better defined events from the August 2004 period, yielding estimates for f_o/f_{ce} ranging from 1.06 to 1.20, with an average of 1.13. We also scaled 6 events from the November-December, 2005 period, obtaining estimates for f_o/f_{ce} that ranged narrowly from 1.16 to 1.21, with an average of 1.19.

In none of hundreds of examples of $f_{ce}{}^+$ echoes observed thus far has the constant-delay or hockey-stick part of the echo crossed f_{ce}. Even in the apparently unusual case of Figure 9a there was a 'gap' of $\approx$ 1 kHz between f_{ce} and the echo. We therefore speculate that all discrete echoes above f_{ce} are subject to increasing group delay near f_{ce}, however small the gap may be. This could be true of the ISIS data (referenced above) as well, given the $\approx$ 50-kHz width of the f_{ce} spike on ionograms.

2.2. The $f_{ce}{}^+$ Resonance

As noted, the $f_{ce}{}^+$ resonance appears to be a new phenomenon, not reported from the topside sounder observations near and below $\approx$ 4,000 km. It differs from the discrete $f_{ce}{}^+$ echo in that it can extend from the minimum to the maximum observable range of the plasmagram. We observed this resonance in the plasmasphere from $\approx$ 7,000 km altitude to $\approx$ 20,000 km altitude as f_{ce} varied from $\approx$ 100 kHz to $\approx$ 10 kHz. In the special August 14-22, 2004 period, $f_{ce}{}^+$ resonances were identifiable on 21 of the 114 plasmasphere soundings for which local f_{ce} was in the frequency range being probed. In the months of May, June and July, 2004, an $f_{ce}{}^+$ resonance was detected at least once on 100 of 169 orbits.

The resonances tended to appear within or close to

the frequency range in which $f_{ce}{}^+$ echoes were found, as suggested by Figures 3, 6c, and 6e. Figure 10 is a plot versus log f_{ce} of f_{res}/f_{ce}, the ratio of the $f_{ce}{}^+$ resonance frequency to f_{ce} for observations in a four-month period May-August 2004. The points cluster between 1.05 and 1.20, at ratios similar to the values between 1.1 and $\approx$ 1.25 shown in Figure 7 for $f_{ce}{}^+$ echoes recorded in the August 14-22, 2004 period. The falloff in data points at $f_{ce}= 20$ kHz is attributed to the 20-kHz low-frequency limit of the bulk of the plasmagrams studied. The steep falloff at ≈ 100 kHz is believed to represent a real reduction in occurrence below $\approx 7,000$ km and is consistent with a lack of reports of $f_{ce}{}^+$ resonances from topside sounders operating below 4,000 km altitude.

We find the $f_{ce}{}^+$ echoes and $f_{ce}{}^+$ resonances to be independent phenomena. They both tracked with the local value of f_{ce} and appeared in a similar frequency range above f_{ce}, but were otherwise quite different. While on occasion, as in Figures 3 and 6c above, $f_{ce}{}^+$ echoes appeared to be spur-like attachments on $f_{ce}{}^+$ resonance spikes, as we found to be the case for some Z echoes on f_{pe} resonances (as shown below), in some examples they were observed to cross over the $f_{ce}{}^+$ spike, implying a frequency offset f_o closer to f_{ce} than the resonance spike frequency.

When observed, $f_{ce}{}^+$ resonances tended to differ in appearance from sounding to sounding along a given orbit and from orbit to orbit, being for example weakly defined at 18.5 kHz in Figure 6a, well defined at ≈ 27.5 kHz in Figure 6c, undetectable in Figure 6d, and clearly present but weakly defined at ≈ 47.5 kHz in Figure 6e.

Figures 11a-11d, from an orbit on May 7, 2004, illustrate the appearance of $f_{ce}{}^+$ resonances in the frequency interval 20 - 70 kHz during soundings that extended from 20 to 320 kHz. These soundings, although limited to 1200-Hz frequency steps instead of the 300-Hz resolution provided in Figures 3 and 6, were widely conducted in 2004 outside the special 8-day August interval. In the sequence of Figure 11, the $f_{ce}{}^+$ resonance frequency stayed 10-20% above the f_{ce} spike as altitude decreased from $\approx 16,000$ km (Figure 11a) to $\approx 11,000$ km (Figure 11d). Several changes occurred: the resonance amplitude diminished from Figure 11a to 11b before recovering in plasmagrams 11c and 11d. Bandwidth increased during the sequence; the last two resonances spanned several kHz. Both a wide resonance bandwidth, regularly exceeding 1 kHz, and long persistence, extending to > 320 ms, were indicated in a survey of plasmagrams from 2002 for which frequency was stepped logarithmically at 2% intervals beginning at 50 kHz and for which the maximum detectable time delay was 320 ms.

Spikes that we call $2f_{ce}{}^+$ resonances were sometimes seen slightly above $2f_{ce}$. They were fewer in number, appearing on 6 of the 114 soundings in the special August period. $2f_{ce}$ resonances appeared both in conjunction with a strong $f_{ce}{}^+$ resonance and when only the $2f_{ce}{}^+$ spike was identifiable. An example of the effect is shown in Figure 12. The f_{ce} and $2f_{ce}$ spikes are well defined at 13.2 kHz and 26.4 kHz, respectively, with accompanying resonances at 14.4 kHz and 28.5 kHz. Both resonances were weakly defined until ≈ 20 ms following the leading edge of the sounder pulse.

In Figure 12, note the similarity between the long-range ($t \approx 150$ ms) $f_{ce}{}^+$ echo just to the right of the $f_{ce}{}^+$ resonance spike and the $f_{ce}{}^+$ echo in Figure 6a.

2.2.1. Amplitude Variations in $f_{ce}{}^+$ Resonances

Unlike the nf_{ce} resonances, which usually tapered off in amplitude as time increased, the $f_{ce}{}^+$ resonances tended to remain strong up to the maximum observable

delay of 178 ms (in the 2004 data) and 320 ms (in the 2002 data). On occasion they were relatively weak during the first ≈ 20 ms after the transmitter pulse, as illustrated by the $2f_{ce}{}^+$ resonance in Figure 12 (a similar but much shorter (≈ 1 ms) 'float' above the base line was reported by *Hagg and Muldrew* [1970] in connection with a resonance on Alouette 2 at $f_{uh}/2$). At times they were skewed in the first ≈ 20 ms toward frequencies ≈ 1 kHz higher, as illustrated in Figure 12 by the $f_{ce}{}^+$ resonance.

Although the $f_{ce}{}^+$ resonance was found to track with the local value of f_{ce}, in most cases we observed no obvious connection to the local value of t_p. However, Figures 11b and 11c show fragmentation of the resonance at short delay times. Some of these low-range drop-outs appear to be the result of interference by PGH echoes, since the time delay during the drop-out coincides with a multiple of t_p, as illustrated in Figure 13. An example was found in which the $f_{ce}{}^+$ resonance weakened periodically at the delays of a sequence of WM echoes, as illustrated in Figure 14 by a 3D amplitude plot (and by a plasmagram in the WM section below). In this case, as the WM echo amplitude decreased at higher multiples of t_p, the correlated perturbations of the resonance became less pronounced.

2.2.2. Factors Affecting $f_{ce}{}^+$ Echo and Resonance Occurrence

How are the observed properties of $f_{ce}{}^+$ echoes and resonances related to: (1) local plasma density, (2) the orientation of the RPI antennas with respect to $\mathbf{B}$, (3) the angle ϕ between the IMAGE velocity vector $\mathbf{V_S}$ and $\mathbf{B}$? In past work with topside ionosphere records, both antenna orientation and the angle ϕ were found important. For example, *King and Preece*, [1967] found that proton gyroharmonic spurs on electron resonance spikes occurred most frequently when the satellite antenna was parallel to Earth's magnetic field $\mathbf{B}$. In addition, *Oya* [1978] found that PGH echo occurrences in the Alouette 2 data were concentrated in near-equatorial regions where the satellite velocity vector was close to the direction of $\mathbf{B}$.

Thus far we have not found a clear dependence of $f_{ce}{}^+$ echo and resonance activity on antenna angle, and within the altitude range where $f_{ce}{}^+$ echoes and resonances are observed, have not found a clear dependence upon plasma density. However, occurrences of both phenomena decreased as the average angle ϕ between $\mathbf{V_S}$ and $\mathbf{B}$ increased. Data from June 2004 and July 2005 were compared. The sounding schedules in the two periods were similar, but the orbital inclinations were such that in 2004 the mean value of ϕ at altitudes near 12,000 km was $\approx 20°$, as compared to $\approx 60°$ in 2005. In June, 2004, $f_{ce}{}^+$ resonances were seen on 39 orbits, while in July, 2005 they were identified on only 8 orbits. Similarly, $f_{ce}{}^+$ echoes were detected on 27 orbits in June 2004 but on only 10 orbits in July, 2005. Thus there was a clear velocity vector effect, but it was not as strongly peaked at low values of ϕ as was the topside sounder activity reported by *Oya* [1978]. In fact, in various 2005 data periods we found well-defined examples of both $f_{ce}{}^+$ resonances and $f_{ce}{}^+$ echoes when the angle ϕ was close to $90°$.

Variations in $f_{ce}{}^+$ resonance and echo activity with ϕ involve questions of accessibility; for large ϕ IMAGE would move a distance of order 500 m transverse to $\mathbf{B}$ during the 80 - 100 ms before a typical $f_{ce}{}^+$ echo could be received in the outer plasmasphere. This would appear to place the satellite at the outer limits of the region occupied by sounder-accelerated protons. The gradual rather than steep falloff of PGH activity with ϕ suggests that

the effective size of the region heated by an individual sounding pulse was several hundred meters, substantially larger than the several meters normally associated with a plasma sheath around an electric antenna at a voltage of $\approx$ 100 V. Our observations of echoes at large ϕ may also have occurred because on occasion the rotating 250-m RPI antenna segments (one partially truncated) was favorably positioned with respect to the wave 'source'.

2.3. WM Echoes

At altitudes below $\approx$ 12,000 km, discrete PGH echoes in the whistler-mode domain were detected on essentially every orbit surveyed. In some cases, the echoes appeared on plasmagrams showing other PGH echo activity, as illustrated in Figures 3 and 4. WM echoes were seen down to the lowest altitudes reached in the plasmasphere, $\approx$ 1,500 km.

Since WM echoes are a very low frequency (VLF) phenomenon, they were most readily detected by sounding programs that extended well below 50 kHz, such as the 6-63 kHz program illustrated in Figure 3 and also an earlier program that swept in steps of 300 Hz from 7 kHz to 19.9 kHz. Figure 15 shows in meridian-cross section the locations where WM echoes were recorded during two periods, November 1 - 20, 2001 and August 14 - 22, 2004. The locations in 2004 were all in the northern hemisphere, those from 2001 all in the southern hemisphere.

Most of the WM echoes observed thus far were found within the plasmasphere or the PBL at magnetic latitudes between -60° and 60°. They were evident on occasion at higher latitudes and over the polar regions, but tended to be obscured there by strong natural whistler-mode noise with power spectral density 10 dB or more above the noise levels in the plasmasphere. Our samplings showed strong WM echo activity at several widely spaced magnetic local times, suggesting that such echoes may occur in all local time sectors.

At each frequency during a given sounding, WM echoes tended to repeat at time delays that were multiples of t_p. Figures 16a to 16c display such effects on plasmagrams recorded on three different orbits at altitudes $\approx$ 10,700 km, $\approx$ 7,700 km, and $\approx$ 4,200 km, respectively. As altitude decreased, the inter-echo time delay decreased accordingly. Note that the event in Figure 16a was shown from a 3D perspective in Figure 14a. In the case of Figure 16c, discrete echoes up to 18th order were detected.

In the stronger magnetic fields below $\approx$ 3,000 km altitude, the time interval at each frequency between successive high-order echoes fell below 6.4 ms, the minimum interval allowing separation of echoes by one 3.2-ms time-delay pixel, and individual echoes could no longer be resolved. In such cases, the echoes formed a 'continuous' response extending to multiple values of t_p, as in the example of Figure 17. In this case IMAGE was in the plasmasphere boundary layer at L $\approx$ 4.9 at an altitude of 1,750 km and at $\approx$ 58° magnetic latitude, prior to being blanketed at the frequencies of interest by auroral whistler-mode noise. This sounding may be compared with that of Figure 16c, which occurred $\approx$ 13 min earlier on the same orbit (note the different time-delay scales).

In Figure 17 the time-compressed PGH echo activity was accompanied at longer delays by discrete whistler-mode echoes that are interpreted as having returned to IMAGE after reflection from the lower boundary of the underlying ionosphere [*Sonwalkar et al.*, 2003].

In Figure 18 we plot the delay time t_{min} of the initial or lowest-delay WM echo versus the local proton gyrofrequency f_{cp}. As in Figure 8, the solid curve repre-

sents the simple inverse relationship between the proton gyroperiod t_p and f_{cp}. It is clear that the observed WM echo delays were controlled by proton dynamics in the vicinity of the satellite.

With each successive higher-order echo in a WM event, the frequency range of detectability over the noise background tended to narrow, as indicated in Figures 16a, 16b, and 16c, often converging to a value between 8 and 12 kHz. Figure 19 is a histogram of the number of echoes for each frequency between 6 and 20 kHz for the above-mentioned periods in November 2001 and August 2004, taking account of echoes of all order. An echo was determined to be present if its amplitude exceeded that of the noise by 10 dB. It is not known why there are two peaks fairly close in frequency instead of a single peak. The overall falloff in echo activity with frequency above ≈ 10 kHz is discussed further below.

The number of higher-order WM echoes near 10 kHz was found to reach a maximum as ϕ passed through a minimum value, typically increasing from 2 or 3 at an angle of $\approx 40°$ to 10 or more as the angle reached a minimum value of $\approx 10°$. We have not yet found a dependence of WM echo order on the antenna angle with respect to **B**.

2.3.1. Amplitude Profile of a WM Echo

From study of the amplitude-versus time profile of a series of WM echoes at a given frequency near 10 kHz, we can estimate that the profile of the first echo contains a single narrow peak centered approximately at t $= t_p$. This peak is identified from sounding records on which a sequence of discrete echoes at a given frequency near 10 kHz is nearly 'synchronous' in time with the RPI receiver data samples at that frequency. That is, $t_{i(echo)} \approx (n)x(3.2ms)$ and signal levels in time bins next to the principal echo elements are either at background levels or from 15 to 20 dB below the levels in the principal echo bins. A simple backward extrapolation of such an echo series in time would lead to a 3.2-ms interval centered at $t = 0$. However, since the initial 3.2 ms rf pulse only begins at $t = 0$, the echo series is considered to be dominated by a transient reponse at the pulse leading edge.

The apparent temporal broadening of WM echoes near 10 kHz on some records, such as in Figure 11c, is not fully understood. Possible contributions come from saturation of the receiver by the lower-order echoes, time delay broadening of the echo peaks with increasing echo order, and enhanced whistler-mode noise near the lower hybrid resonance frequency $f_{lh} \approx f_{ce}/43$ which is ≈ 7 kHz at the altitudes in question.

2.3.2. Estimated Size of the Perturbed Region

From knowledge of the satellite velocity, the angle ϕ, and the duration of WM echo activity at a fixed frequency near 10 kHz, we can estimate the distance Δ transverse to **B** within which WM echoes were observed. On a given orbit in October, 2005 there were typically five successive soundings with identifiable echoes. As noted above, the number of high-order echoes varied inversely with the angle ϕ, so that Δ typically remained in the range 100–300 m during the sequence of soundings. From the ten orbits in October, 2005 with the maximum number of 10-kHz echoes, we found that the average time delay to the highest-order echo detectable was 120 ms, the average spacecraft velociy was 7.6 km/s, and the average angle ϕ was 11°, giving a value of $\Delta \approx 170$ m. This value is consistent with the several-hundred meter transverse scale size of the region in which f_{ce}^+ echoes were detected. After emitting the intial rf pulse and while still within Δ m of the original field line, the satellite moved ≈ 800 m in the **B** direction.

2.4. Z Echoes

The PGH Z echo, like the WM echo and the lowest-time-delay part of the $f_{ce}{}^+$ echo, occurs at a delay equal to the proton gyro-period (within the uncertainty imposed by the 3.2-ms length of the sounder pulse). Such echoes could be observed whenever the upper limit of the non-propagation band of Figure 1 was being covered by the sounding program in use. The activity of Figure 4 occurred as IMAGE was beginning to move outward into the PBL and into the low-altitude polar region. Typically, the detected low-frequency limit of the Z echo was in that part of the no-propagation domain extending $\approx$ 20-30 kHz below f_Z, which in this case was $\approx$ 304 kHz. As noted in Figure 4, the Z echo was particularly strong above f_Z, where it appeared against a Z-mode noise background that was $\approx$ 20 dB above the background below f_Z.

Figures 20a through 20c show examples of Z echoes recorded on an orbit on August 14, 2005 as IMAGE was moving outward through the plasmasphere at altitudes ranging from $\approx$ 7,600 km to $\approx$ 11,800 km. Time delay from 0 to 128 ms is displayed versus sounding frequency from 200 to 326 kHz. The delays of the Z echoes increased with altitude, as expected. In these cases the echoes displayed some time-delay spreading, not unlike that reported for spurs on topside sounder resonances, for example by *Benson* [1975] and *Horita* [1987]. In particular, the event of Figure 20c, recorded at L $\approx$ 2.8, shows spur-like spreading toward a resonance at $f_{pe} \approx$ 257 kHz. This resonance was approximately coincident with the seventh harmonic of f_{ce} at 255 kHz, a result consistent with *Benson*'s [1975] finding from Alouette 2 data that some of the best-defined PGH spurs appeared when f_{pe} was an approximate multiple of f_{ce}.

Thanks to a reduction from 12.4 ms to 6.4 ms in the minimum time delay displayed on RPI plasmagrams from 2005, it was found that PGH Z echoes at a given range of frequencies were regularly accompanied at shorter delays (beginning at the minimum detectable time delay of 6.4 ms) by intense Z-mode echoes, often at levels that saturated the receiver. This could occur at frequencies below f_Z, as in Figure 20a, but was most commonly present above f_Z, as in Figure 20c. The low range echo activity was particularly evident on the short (20-m) Z antenna (not illustrated here). It is interpreted as the result of scattering from field-aligned density irregularities in the near vicinity of IMAGE, a phenomenon of RPI data recently investigated by *Sonwalkar et al.* [2003].

3. Discussion

In addition to being dependent upon the proton gyrofrequency f_{cp}, each of the four categories of PGH echo forms was closely associated with one or two particular plasma parameters. In the case of the $f_{ce}{}^+$ echoes and resonances it was the electron gyrofrequency f_{ce}, in the WM case (as discussed below) the proton plasma frequency, and in the Z-echo case, the Z-mode cutoff f_Z and the electron plasma frequency f_{pe}.

3.1. PGH Mechanisms: WM Echoes
3.1.1. A Quasi-Electrostatic Mechanism

The observations suggest that WM echoes consist of a series of quasi-electrostatic noise bursts due to a periodic spatial bunching of ambient protons that have been energized at the leading edge of each 3.2-ms rf antenna pulse. The noise bursts are not replicas of the initiating pulses, but they do depend weakly upon the pulse rf frequency.

The proton energization occurs during a transient phase when a positive potential is first applied to one of the IMAGE dipole antenna elements and an electron sheath begins to form about the positive antenna element. The ambient electrons respond quickly to the impressed electric field produced by the positive potential and flow towards the positive antenna element. The ambient protons, on the other hand, because of their much larger mass, take a much longer time to leave the region of positive potential. Thus the time necessary to form a complete electron sheath around the positive element depends upon the initial energization of the ambient protons. The transient acceleration period ends when the ambient protons initially surrounding the antenna have been accelerated radially outward sufficiently so that the electric field due to the electron space charge now surrounding the positive element cancels the electric field due to the positive potential applied to the antenna element. The ambient protons initially closest to the positive antenna element will be accelerated more than those initially located farther from this element, with the protons initially closest to the antenna gaining energies up to 400 eV and those initially farther away gaining as little as ~ 1 eV. Thus, as the radial acceleration proceeds, the energized protons undergo spatial bunching [*Calder and LaFramboise*, 1990].

When the bunched protons leave the edge of the sheath region, they follow orbits dictated by the effects of their own self-electric field as well as the Earth' magnetic field. We assume that the energized proton's self-field will be neutralized by thermal electrons flowing along B_o. In this case the protons move along cyclotron orbits primarily under the influence of B_o, as illustrated in Figure 21. Because the energized protons have a wide range of energies from 1 - 400 eV, the gyro-radius of the protons will also have a wide range. For example, at $L \simeq 2$ near the magnetic equatorial plane, the gyro-radius of the protons ranges from ~ 50 - 800 m. Thus after one half gyro-period, the protons are well removed from the antenna and their number density and self field are greatly reduced.

Now consider the special case in which the antenna is parallel to B_o when the positive potential is applied to the antenna element. After one complete gyro-period, the energized protons return to the magnetic field line on which they were located when they first left the sheath region (for example, the magnetic field line through point P_1 in Figure 21). Due to their original thermal velocity along B_o, the returning protons will be spread over a distance δs along B_o of approximately: $\delta s = l + 2\,v_{mp}\,t_p$, where l is the antenna element length, v_{mp} is the most probable velocity of the protons along B_o, and t_p is the proton gyro period, as illustrated in Figure 22.

For an initial proton temperature of $4000°$ K, $v_{mp} \simeq 4$ km/s, and if $t_p \simeq 20$ ms, $\delta s \simeq l + 160$ m. Since $l = 250$ m, the spread of the protons along B_o during the first gyro period is relatively small, and the self field of the protons will not differ significantly from the self field that existed at the end of the original transient period when the protons were bunched near the sheath boundary. Because of the thermal spread along B_o, the average number density of the protons will decrease with time as $(l + 2\,v_{mp}\,t_p)^{-1}$. After each succeeding gyro-period, the energized protons bunch once again on their initial magnetic field line but are spread more and more widely along B_o. Thus after m gyro-periods, the energized protons form a thin shell of charge symmetrically distributed about the magnetic field line on which the positive antenna element was initially located.

Thermal electrons cannot follow the energized protons across B_o because of the small gyro radius of these electrons. Consequently, they can neutralize the self-electric field of the protons only by moving along B_o. The minimum time necessary to neutralize the proton self-field is roughly equal to the antenna length l divided by the electron thermal velocity v_{th} along B_o. For our parameters, assuming an electron temperature of $4000°$, $l/v_{th} \sim 0.5$ ms. Thus the self-field $E_s(r,t)$ of the energized protons has a temporal behavior resembling a delta function. We can approximate the proton self-field by the expression:

$$E_s(r,t) \simeq \Sigma E_{sm}(r)\,\delta(t - m\,t_p)$$

where $E_{sm}(r)$ is the normalized proton self field that exists in space at gyro period m.

The magnitude of $E_s(r,t)$ can be quite large. For example when the antenna driving frequency is near 10 kHz, calculations indicate that the magnitude of the proton self field at the first gyro period exceeds 20 mV/m in a 500 m region surrounding the original location of the positive antenna element. Electric fields of this magnitude can easily produce antenna voltages sufficiently large to saturate the RPI receiver. Since the IMAGE spacecraft velocity is approximately 7 km/s in the region of interest, the spacecraft remains within this high E field volume for many gyro periods.

The key feature of this mechanism is the fact that the energized protons are tightly bunched in space after every gyro period. This tight bunching of the protons can only occur during the transient period when the electron sheath is formimg. At that point, the ambient protons possess thermal energy which is very small compared to the energy that they acquire during the sheath formation period and can thus be tightly bunched as they move outward. The situation is quite different during the rest of the 3.2-ms transmission period. For example, at the beginning of a positive voltage cycle for a given antenna element, the protons surrounding the element are those that have been accelerated toward the element during the previous negative voltage cycle. These protons have a wide range of energies and directions, and thus are not significantly bunched as they leave the sheath region.

As shown in the Appendix, Section 5.2, the transient energization of the ambient protons initially near the antenna is a function of the ratio of the frequency f of the applied antenna voltage to the proton plasma frequency, f_{pp}. If $(f/f_{pp})^2 \ll 1$, the protons exit the sheath before the antenna voltage reaches its peak. Because the voltage at that point is smaller, the energization and bunching of the protons is reduced in magnitude and the self electric field of the protons is diminished. If $(f/f_{pp})^2 \gg 1$, the antenna voltage will change from positive to negative before the protons can leave the sheath, and thus their energization and bunching will be limited.

This mechanism can explain the occurrence of peaks in the WM echoes at multiples of the local value of t_p following the leading edge of the rf pulse. Since at the altitudes of WM echo observations the value of f_{pp} varies between ≈ 6 and 13 kHz, it can also explain the high amplitude of WM echoes near and below 10 kHz, frequently saturating the receiver, as well as the drop-off in high-order echo activity between 10 kHz and ≈ 50 kHz, summarized in Figure 19 and illustrated in Figures 16b, 16c, and 17. It is also consistent with the lack of WM activity above $\approx 11,000$ km altitude, where the value of f_{pp} falls below the 6-kHz lower operating limit of RPI.

In our analysis above we have considered only the case in which the RPI antenna is parallel to B_o. The situation is much more complicated when the antenna is not

parallel to B_o during transmissions. In this case, the majority of the most highly energized protons rapidly leave the vicinity of the antenna, and only the lower energy protons are left to create a significant self field. The self field that is created is not symmetric about B_o. Because of these complications, further analysis of this case is beyond the scope of the present paper.

3.2. PGH Mechanisms: f_{ce}^+ Echoes

Unlike WM echoes, f_{ce}^+ echoes exhibit a clear frequency dependence, suggesting the possibility that they propagate from a perturbed proton distribution in thermal wave modes, in the manner discussed by *Muldrew* [1998] when interpreting topside sounder observations of echoes above f_{ce}. However, it is not clear how the perturbed proton distribution is created. f_{ce}^+ echoes occur at high ratios of f/f_{pp}, implying that they do not originate in the energization processes that give rise to the high amplitude WM echoes. It is possible that f_{ce}^+ echoes are detectable because the energization process involved occurs in a nominally non-propagating frequency domain, where the background noise levels are 20 to 30 dB below those present at the frequencies of WM events.

One source of free energy available to drive the f_{ce}^+ echoes resides in the electric field in the plasma sheath which surrounds each antenna element after each 3.2-ms transmitter pulse. During each pulse, the antenna acquires a net negative charge from the plasma because the mobility of the electrons accelerated toward the positive-voltage antenna element during each half rf cycle is much greater than the mobility of the ions accelerated toward the negative-voltage antenna element.

The net negative charge acquired by the antenna during each 3.2-ms transmitter pulse is approximately twice the negative charge that initially appeared on the negative antenna element at the start of the pulse [e.g., *Oya*, 1978]. Consequently, when the transmissions cease, each antenna element carries a net negative charge. This negative charge produces an electric field that repels electrons and attracts ions, creating an ion sheath around each antenna element. The negative charge on the antenna elements will eventually be neutralized by the ion flux accelerated toward the antenna, but since the ion mobility is relatively small, this neutralization requires a time that is generally much larger than the 3.2-ms transmission time (see Appendix). During the time the ion sheath exists, the sheath electric field represents a free energy source which may be partially responsible for driving the weaker PGH phenomena.

3.3. PGH Mechanisms: f_{ce}^+ Resonances

The mechanism of f_{ce}^+ resonances appears to operate independently of the f_{ce}^+ echo mechanism, although both phenomena occur within a similar range of frequencies above f_{ce}. A key difference may be that the resonances have not been reported below $\approx$ 7,000 km altitude, while f_{ce}^+ echoes can be present at ionospheric heights. The long enduring nature of the resonances, lasting at times for at least 300 ms, suggests that the perturbed plasma environment in which they occurred was carried with the spacecraft well beyond the $\approx$ 300 m transverse distance within which, for example, the WM echoes were found to be confined. In seeking an as yet unspecified mechanism of the f_{ce}^+ resonances, one must consider the occasional 20 to 30 ms delay in their rise to peak amplitude as well as cases in which the frequency is initially skewed to higher values before settling. One possible source of energy for the resonances lies in the

collapse of the ion sheath discussed above.

3.4. PGH Mechanisms: Z Echoes

In interpeting Z echoes we need to consider: (i) evidence of temporal broadening and spur-like form at or near the f_{pe} resonance, (ii) appearance both above and below f_Z, and (iii) evidence that Z echoes are accompanied at shorter delays by the launching of strong Z-mode waves by RPI, some of which are scattered and return at high amplitude to the antenna.

4. Concluding Remarks

We find that when the RPI operated between $\approx$ 1500 km and 20,000 km altitude in the plasmasphere, information about its 3.2-ms-long rf pulses was stored in the surrounding proton plasma and returned in a variety of echo forms to the spacecraft. Some of the echo forms are similar to signatures reported earlier from ISIS-series sounding at altitudes below $\approx$ 3,000 km. As in the ISIS-series work, we observed discrete echoes in a non-propagating frequency domain above the electron gyrofrequency f_{ce}. The echoes arrived at delays equal to the proton gyroperiod t_p (and on occasion at multiples of t_p), although their delays could be substantially longer than t_p within a narrow band just above f_{ce} . Also, as in the ISIS work, we observed spurs, variously shaped broadenings at multiples of t_p along resonance spikes such as the plasma frequency f_{pe}.

The RPI data exhibited a new effect not found in topside sounder records, a resonance at a frequency $\approx$ 15% above f_{ce}. Occasionally a similar resonance appeared just above $2f_{ce}$. Resonances were detected from $\approx$ 7,000 km altitude to $\approx$ 20,000 km altitude, and in some months were found at least once on over half the IMAGE orbits through the plasmasphere. The $f_{ce}{}^+$ resonance was often poorly defined or skewed in frequency during an initial delay of order 20 ms, in contrast to most resonances familiar from topside sounding, which begin at or near maximum amplitude. The $f_{ce}{}^+$ resonance was not tapered, as were the usual nf_{ce} spikes, but regularly remained at or near full amplitude to the time limit of the plasmagram, which in some cases reached $\approx$ 300 ms. Occasional evidence was found of decreases in resonance amplitude at multiples of t_p.

The most intense and most frequently observed PGH events, called WM echoes, appeared in the whistler-mode domain between $\approx$ 6 and 50 kHz, with a peak in occurrence and intensity near 10 kHz. WM echoes were detected at altitudes below $\approx$ 12,000 km on essentially every IMAGE orbit. They were usually followed by additional discrete echoes, sometimes as many as 15 or more, at multiples of t_p. At altitudes below $\approx$ 3,000 km the individual WM echoes could no longer be resolved because t_p fell below 6.4-ms, the minimum interval separating resolvable echoes. The echoes then appeared on plasmagrams as a continuous return, often extending to $\approx$ 10 t_p at the most active frequencies near 10 kHz.

Time delay measurements of WM echoes near 10 kHz indicated that the energization of the protons by a given 3.2-ms sounder pulse was essentially a transient process that occurred at the beginning of the pulse, and to that extent did not involve replication of the pulse rf frequency by the echo. We concluded that the WM echo mechanism was quasi-electrostatic in nature, with spatial bunching of protons during the first positive rf half cycle on one of the antenna elements, such that a high voltage was induced in the RPI antenna at multiples of t_p after t = 0. The high intensity of the lower-order WM

echoes, which regularly saturated the RPI receiver near 10 kHz, as well as the lack of detectable WM echo activity above 12,000 km altitude, are attributed in part to the fact that proton energization at the leading edge of the sounder pulse was at maximum levels when the rf of the pulse was below, but near, the local proton plasma frequency $f_{pp} = f_{pe}/43$. f_{pp} reaches a maximum of ≈ 13 kHz at the lower IMAGE altitudes, but falls below 6 kHz (the lowest sounder operating frequency) above 12,000 km.

The $f_{ce}{}^+$ echoes occur at frequencies well above f_{pp} and hence well outside the range where significant transient energization is expected. In contrast to WM echoes, $f_{ce}{}^+$ echoes replicate the sounder pulse frequency and in so doing experience large frequency-dependent increases in travel time as f_{ce} is approached from above. We are challenged to understand the offset effect, a gap between f_{ce} and a higher frequency at which a dispersed $f_{ce}{}^+$ echo appears to develop an asymptotically long time delay. We need to discover what geophysical parameters, among them electron temperature, may be important in the $f_{ce}{}^+$ echo process and might provide a basis for future diagnostic use of PGH echo phenomena, a topic pursued in the work of *Muldrew* [1998]. A possible source of energy for the comparatively weak $f_{ce}{}^+$ echoes is the collapse of the ion sheath that surrounds each antenna element in the immediate aftermath of an rf pulse, as discussed in the Appendix, Section 5.1.

The mechanism of $f_{ce}{}^+$ resonances appears to operate independently of the $f_{ce}{}^+$ echo mechanism, although both phenomena occurred within a similar range of frequencies above f_{ce}. In contrast to the $f_{ce}{}^+$ echo, which has been observed from topside sounders, the $f_{ce}{}^+$ resonance appears to be restricted to altitudes above $\approx 7,000$ km. The long enduring nature of the resonances, lasting at times for at least 300 ms, suggests that the perturbed plasma environment in which the ringing occurred was carried with the spacecraft a kilometer or more beyond the ≈ 300 m transverse distance within which the WM echoes were found to be confined.

The Z echoes appear to benefit from, or be coincident with, efficient excitation of normal Z-mode waves by the sounder in a range between f_Z and the electron plasma frequency. Strong Z echoes above f_Z are often accompanied at shorter time delays (beginning at the lowest measurable delay of 6.4 ms) by high amplitude Z-mode waves that have been scattered from nearby field-aligned density irregularities.

Earlier workers shed light on what we believe to be important elements in the PGH echo process, among them the accumulation of negative charge on an antenna during an rf pulse [*Oya*, 1978], Bernstein-mode propagation at frequencies above f_{ce} from an excited proton population [*Muldrew*, 1998], and the observation that PGH spur effects on the electron plasma frequency resonance are enhanced when f_{pe} is an approximate multiple of f_{ce} [*Benson*, 1975].

5. Appendix

5.1. Antenna Discharging Time

During transmission of 3.2 ms pulses from RPI, both elements of the dipole antenna will acquire a negative charge because of the much greater mobility of the electrons. When transmissions cease, this negative charge is slowly neutralized by a flux of protons that moves through the sheath and impacts the antenna surface. As a result of the proton flux, the time rate of increase of antenna charge per unit length has the value:

$$\frac{dQ}{dt} = \pi a e N_p \sqrt{2e|V_a|/m_p} \qquad (A1)$$

where a is the antenna radius, e is the magnitude of the electron charge, V_a is the antenna voltage, N_p is the ambient proton number density just outside the sheath, and m_p is the proton mass. We can express the antenna voltage V_o as a function of Q through the relation:

$$Q = CV_a \qquad (A2)$$

where C is the antenna capacitance per unit length. Assuming that end effects can be neglected, the antenna capacitance per unit length can be expressed in terms of the sheath radius r_s:

$$C = 2\pi\epsilon_o / \log(r_s/a) \qquad (A3)$$

where ϵ_o is the permittivity of free space. Since C depends upon r_s and r_s depends upon V_a, we cannot directly solve for $Q(t)$ using (A1), (A2), and (A3).

To relate the variables, we assume that the sheath is cylindrically symmetric about the antenna element, and note that since the RPI transmitting antenna radius is very small ($a = 0.2$ mm), it will collect only a small proton current from the sheath. Under these conditions the density of protons within the sheath will be approximately constant and equal to the ambient proton density [*Laframboise and Rubinstein*, 1976]]. To relate the variables, we solve Poisson's equation:

$$\nabla^2 \Phi(r) = -e\, N_p/\epsilon_o \qquad (A4)$$

where $\Phi(r)$ is the potential function, and we use the boundary conditions $\Phi(a) = V_a$ and $\partial\Phi(r)/\partial r = 0$ at $r = r_s$. Under these conditions $\Phi(r)$ has the form:

$$\Phi(r) = V_a + \frac{eN_p}{2\epsilon_o}[r_s^2 \log(r/a) - \frac{1}{2}(r^2 - a^2)] \qquad (A5)$$

At this point we can implicitly define r_s by requiring that $\Phi(r_s) = 0$. This leads to the following relation between V_a and r_s [*Mlodnosky and Garriot*, 1963; *Linson*, 1969]:

$$|V_a| = \frac{eN_p}{2\epsilon_o}[r_s^2 \log(r_s/a) - \frac{1}{2}(r_s^2 - a^2)] \qquad (A6)$$

We can use (A6) to find an average value of C, C_a, over the voltage range of interest. Then C_a can be used in (A1) and (A2) in order to estimate the discharge time of the antenna. In determining C_a, it should be noted that the minimum value of the quantity $|eV_a|$ is approximately equal to the thermal electron temperature expressed in electron-volts, and the minimum value of r_s is approximately equal to the Debye length. Using C_a, the discharge time can be written:

$$t_d = C_a \sqrt{2e|V_o|/m_p} /(a f_{pp}^2 4\pi^3 \epsilon_o) \qquad (A7)$$

where V_o is the initial antenna voltage, and f_{pp} is the proton plasma frequency.

In general t_d is of the order of 100 ms. For example at $L \simeq 2$ near the magnetic equatorial plane, assuming $N_o \simeq 3000/\text{cm}^3$ and $|V_o| \simeq 400$ V, we find that $C_a \simeq 4$ pF/m and $t_d \simeq 90$ ms. The discharge time will be shorter in general if the protons which impact the antenna eject secondary electrons.

5.2. Proton Transit Time Across the Sheath

The RPI instrument applies a sinusoidal voltage to the antenna which varies as $V(t) = V_a \sin(2\pi f t)$, where

$V_a = 400$ V. To estimate the minimum transit time δt of an ambient thermal proton from a position near the positive antenna element to the sheath edge, we assume that the antenna voltage is applied as a step function in a time which is small compared to δt. In this case the radial kinetic energy of such a proton is governed by the relation:

$$\frac{1}{2} m_p \left(\frac{dr}{dt}\right)^2 = \frac{1}{2} m_p v_r^2 + e\left[V_a - \Phi(r)\right] \qquad (A8)$$

where v_r is the magnitude of the initial thermal radial velocity of the proton. Using (A8), the proton transit time δt from a to r_s can be written:

$$\int_a^{r_s} \frac{dr}{\sqrt{2e|V_a - \phi(r)|/m_p + v_r^2}} = \delta t \qquad (A9)$$

We note that the proton plasma frequency f_{pp} is defined by the relation: $f_{pp}^2 = q^2 N_o/(4\pi^2 \epsilon_o m_p)$. Using this fact we can express (A9) in the following form:

$$\int_a^{r_s} \frac{2\pi dr}{\sqrt{r_s^2 \log(r_s/r) - \frac{1}{2}(r_s^2 - r^2) + \lambda_d^2}} = f_{pp} \, \delta t \quad (A10)$$

where $\lambda_d = v_r/2\pi f_{pp}$ is the Debye length at the sheath edge. As an example, assume that the proton temperature is 1 eV, that $N_o = 3000/\text{cm}^3$, and that $V_o = 400$ V. In this case, we find that $r_s = 1.3$ m, $\lambda_d = 20$ cm, and $\delta t \simeq (\pi f_{pp})^{-1} \simeq 30\mu$s. A transit time of 30μs is roughly 25% of the 130μs it would take an average thermal proton to cross the same distance. This last fact suggests that the applied voltage must reach its peak value within $\simeq 130\mu$s if the protons are to be significantly energized. A quarter period of $\simeq 130\mu$s corresponds to a driving frequency of $\simeq 2$ kHz. Thus there will be a lower cut off frequency for the ion energization effect.

In addition to the lower cut off frequency for proton energization, there is also an upper cut off frequency. The initial proton energization process becomes much less effective when the appled voltage frequency is so high that ambient protons initially near the positive antenna element cannot cross the sheath before the element acquires a negative voltage and decelerates the protons. We can estimate the frequency f_h at which this effect occurs by approximating the first half cycle of the voltage waveform by a voltage step function whose amplitude is equal to the average voltage over this period, i.e., $V(t) \simeq 2V_a/\pi$. Assuming as before, $V_a = 400$V and $N_o = 3000/\text{cm}^3$, and using these values in (A10), we find $\delta t \simeq 40\mu$s. Thus:

$$f_h \simeq 1/80\mu s \simeq 12\text{kHz} \qquad (A11)$$

It is worthy of note that the proton plasma frequency f_{pp} has a value of 11.4 kHz for $N_o = 3000/\text{cm}^3$. Calculations with different values of V_a and N_o in (A10) yield similar results, and we conclude that transient proton energization at applied voltage frequencies above the proton plasma frequency appears to be less efficient than that produced at lower frequencies. To summarize the above, we expect the PGH effect to weaken both when $(f/f_{pp})^2 \ll 1$ and when $(f/f_{pp})^2 \gg 1$.

References

Benson, R. F. (1975), Ion effects on ionosheric electron resonance phenomena, *Rad. Sci.*, *10*(2), 173–185.

Benson, R. F. (1977), Stimulated plasma waves in the ionosphere, *Rad. Sci.*, *12*(6), 861-878.

Bernstein, I. B. (1958), Waves in a plasma in a magnetic field, *Phys. Rev.*, *109*, 10-21.

Burch, J. L. (2000), IMAGE mission overview, *Space Science Reviews, 91,* 1–14.

Burch, J. L. (2001), Views of Earth's magnetosphere with the IMAGE satellite, *Science. 291*, 541-.

Calder, A. C., and J. G. LaFramboise (1990), Time-dependent sheath response to abrupt electrode voltage changes, *Phys. Fluids B*, 2, 655–.

Calvert, W., and J. R. McAfee (1969), Topside sounder resonances, *Proc. IEEE, 57,* 1019–1024.

Crawford, F. W., and R. S. Harp (1966), Electron cyclotron ehoes from plasmas, *Phys. Lett.*, *21*, 292–293.

Franklin, C. A., and M. A. MacLean (1969), The design of swept-frequency topside sounders, *Proc. IEEE, 57,* 897-928.

Goertz, C. K., and R. J. Strangeway, Plasma Waves, in *Introduction to Space Physics,* M. G. Kivelson and C. T. Russell, eds., Cambridge University Press, 1995.

Hagg, E. L., E. J. Hewens, and G. L. Nelms (1969), The interpretation of topside sounder ionograms, *Proc. IEEE, 57*, 949-959.

Horita, R. E. (1987), Proton-cyclotron echoes and spurs observed on Alouette II and ISIS II, *Rad. Sci.*, *22*(4), 671–686.

King, J. W., and D. M. Preece (1967), Observations of proton gyroeffects in the topside ionosphere, *J. Atmos. Terr. Phys*, *29*, 1387–1390.

Laframboise, J. G., and J. Rubinstein (1976). Theory of a cylindrical probe in a collisionless magnetosplasma, *Phys. Fluids, 19*, pp. 1900-.

Linson, L. M. (1969), Current-voltage characteristics of an electron-emitting satellite in the ionosphere, *J. Geophys. Res., 74*, pp. 2368-.

Mlodnosky, R. F., and O. K. Garriot (1963). The VLF admittance of a dipole in the lower ionosphere, in *Proceedings of the International Conference on the Ionosphere*, The Institute of Physics and the Physical Society, pp. 484-491.

Muldrew, D. B. (1998), Topside sounder proton-cyclotron echo generation from a plasma memory process, *Rad. Sci.*, *33*, 1395-1411.

Oya, H. (1978), Generation mechanism of proton cyclotron echoes due to pulsed radio frequency waves in space plasma, *J. Geophys. Res.*, *83*, 1991-2008.

Reinisch, B. W., D. M. Haines, K. Bibl, G. Cheney, I. A. Galkin, X. Huang, S. H. Myers, G. S. Sales, R. F. Benson, S. F. Fung, J. L. Green, W. W. L. Taylor, J.-L. Bougeret, R. Manning, N. Meyer-Vernet, M. Moncuquet, D. L. Carpenter, D. L. Gallagher, and P. Reiff (2000), The Radio Plasma Imager investigation on the IMAGE spacecraft, *Space Science Reviews, IMAGE special issue*, *91*, 319–359.

Reinisch, B. W., X. Huang, D. M. Haines, I. A. Galkin, J. L. Green, R. F. Benson, S. F. Fung, W. W. L. Taylor, P. H. Reiff, D. L. Gallagher, J.-L. Bougeret, R. Manning, D. L. Carpenter, and S. A. Boardsen (2001), First results from the radio plasma imager on IMAGE, *Geophys. Res. Lett.*, *28*, 1167-.

Tataronis, J. A., and F. W. Crawford (1970), Alouette plasma resonance phenomena, in *Plasma Waves in Space and Laboratory, Proceedings of NATO Advanced Study Institute Roros, Norway*, edited by J. O. Thomas and B. J. Landmark, pp. 91-110, Edinburgh Univ. Press, Edinburgh.

Sonwalkar, V. S., U. S. Inan, T. F. Bell, R. A. Helliwell, V. M Chmyrev, Ya. P. Sobolev, O. Ya. Ovcharenko, and V. Selegej (1994), Simultaneous observations of VLF ground transmitter signals on the DE 1 and COSMOS 1809 satellites: Detection of a magnetospheric caustic and a duct, *J. Geophys. Res., 99*, 17511–17522.

Sonwalkar, V. S., D. L. Carpenter, T. F. Bell, M. Spasojevic, U. S. Inan, J. Li, X. Chen, A Venkatasubramanian, J. Harikumar, R. F. Benson, W. W. L. Taylor, and B.

W. Reinisch (2004), Diagnostics of magnetospheric electron density and irregularities at altitudes < 5000 km using whistler and Z mode echoes from radio sounding on the IMAGE satellite, *109*, A11212, doi:10.1029/2004JA010471.
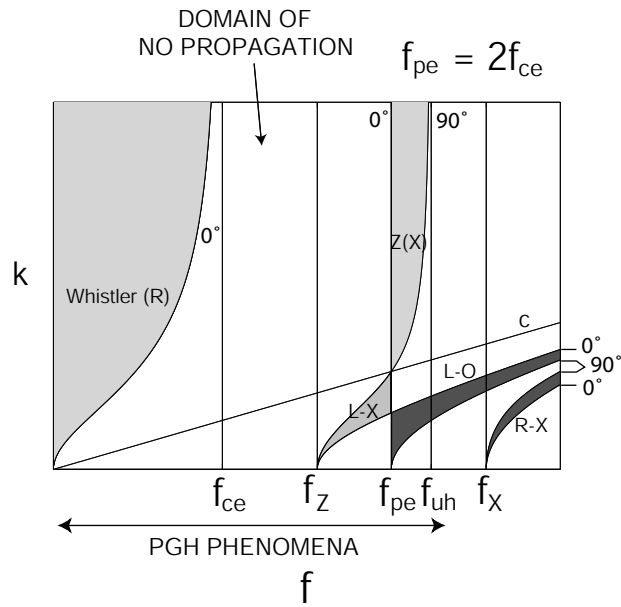
Figure 1. Dispersion diagram for propagation in a cold plasma, with axes reversed so as to display frequency from left to right as it appears on sounder plasmagrams. A ratio of plasma frequency to electon gyrofrequency $f_{pe}/f_{ce} = 2$ was assumed. A horizontal arrow indicates the frequency domains of primary interest in our study. Original diagram adapted from *Goertz and Strangeway*, [1995].
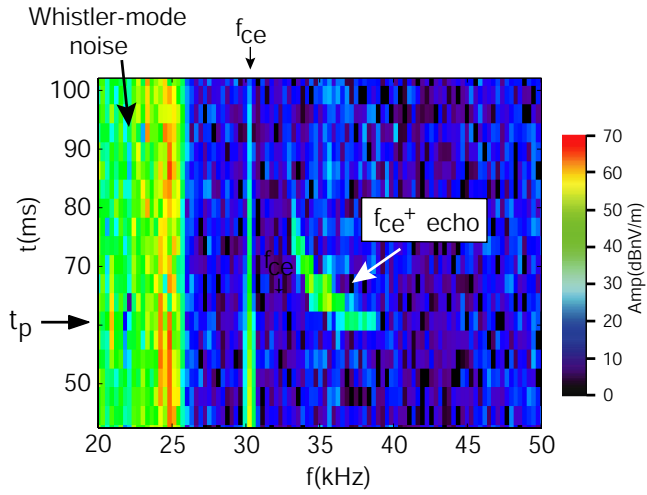
Figure 2. Portion of an RPI plasmagram showing a well defined f_{ce}^+ echo, recorded on August 15, 2004 at 2216:38 UT. Time delay from ≈ 40 to 100 ms is displayed versus sounding frequency from 20 to 50 kHz. The local value of the electron gyrofrequency f_{ce} is marked above the record.
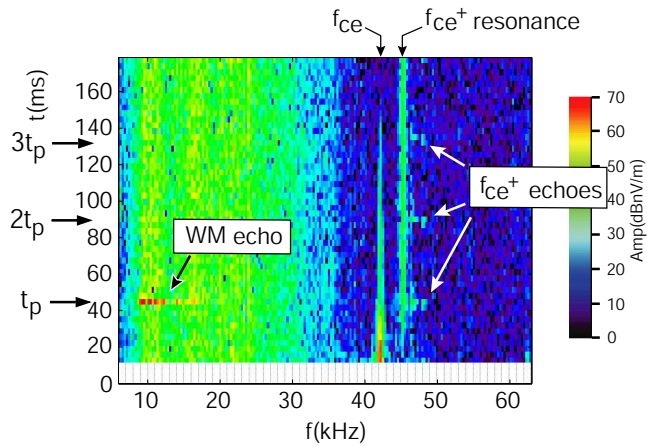
Figure 3. RPI plasmagram illustrating three PGH effects, a WM (whistler-mode domain) echo, f_{ce}^+ echoes, and an f_{ce}^+ resonance. Second and third-order f_{ce}^+ echoes appear at multiples of the local proton gyroperiod t_p. The observations were made on August 14, 2004 at 1757:54 UT.
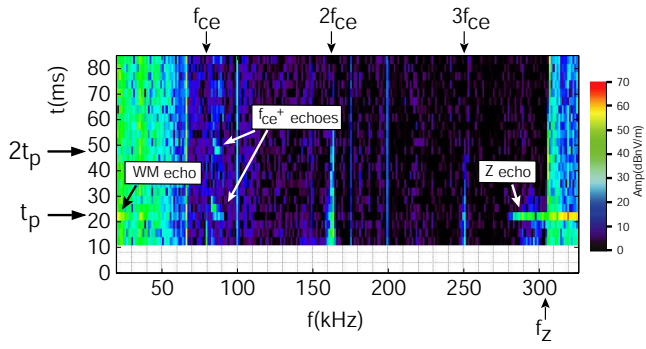
Figure 4. Portion of an RPI plasmagram illustrating three PGH effects, a WM (whistler-mode) echo, f_{ce}^+ echoes, and a Z (Z-mode domain) echo. The sounding program began on September 4, 2004 at 1218:12 UT.
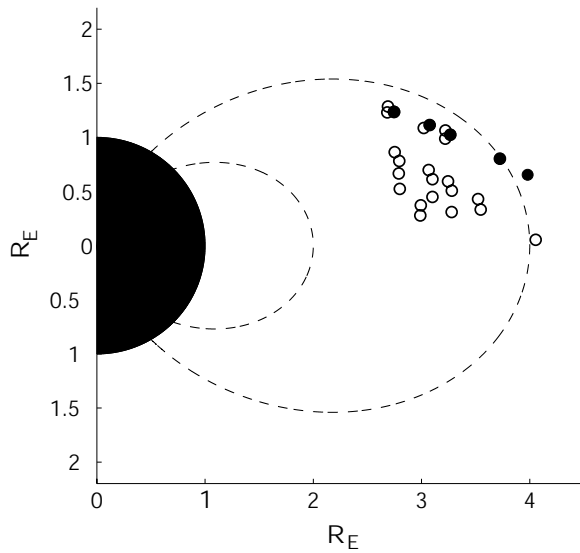
Figure 5. Meridian cross section of the magnetosphere showing the Northern Hemisphere locations along IM-AGE orbits where the most clearly defined c were received during the special period August 14 to August 22, 2004. Filled circles show the locations along an orbit of August 15, 2004 illustrated in Figure 6.
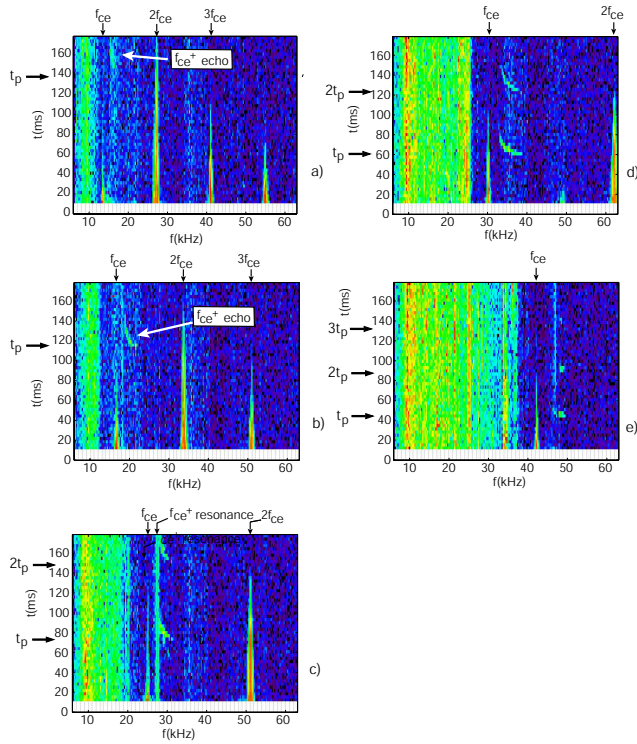
Figure 6. RPI plasmagrams illustrating the variations in $f_{ce}{}^+$ echoes along an IMAGE orbit on August 15, 2004 (see filled-circle locations in Figure 5). (a)–(e) Sequence of soundings at decreasing altitude beginning at 2152:38 UT and ending at 2223:55 UT. Time intervals between the soundings illustrated varied from $\approx$ 5 min to 11 min.
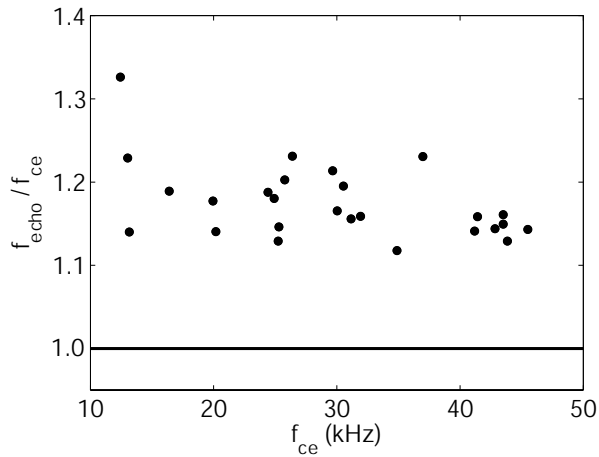
Figure 7. Plot of the ratio of the $f_{ce}{}^+$ echo frequency to f_{ce} versus f_{ce} for the more clearly defined events from the August 14-August 22, 2004 period.
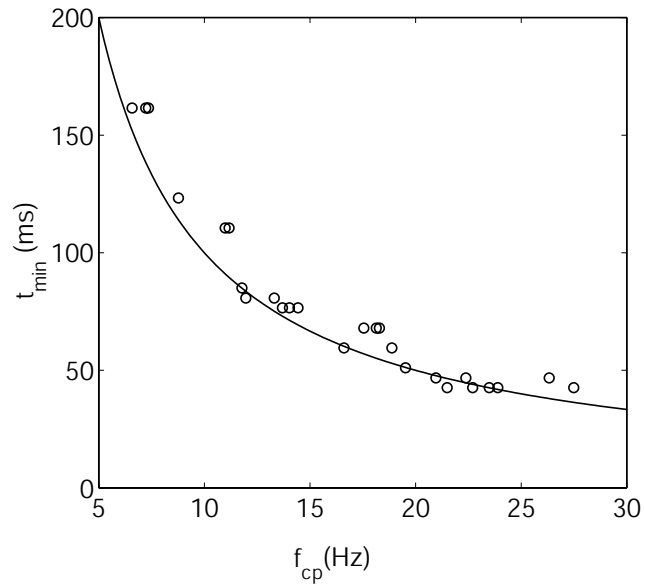
Figure 8. Plot of t_{min}, the shortest detectable echo delay versus f_{cp}, the local proton gyrofrequency, for the f_{ce}^{+} echoes observed in the special August 14-August 22, 2004 period. The solid curve represents the simple inverse relation between t_p and f_{cp}.
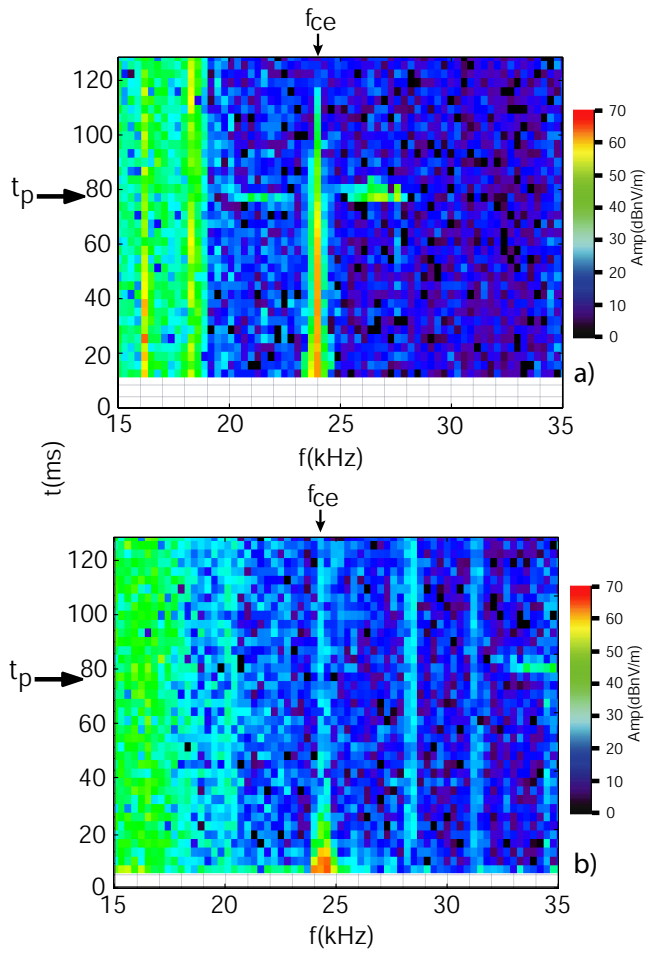
Figure 9. Portions of RPI plasmagrams recorded at two different local times but at similar locations in the plasmasphere, showing examples of f_{ce}^{+} echoes with similar time delays but widely different separations from f_{ce} in frequency. (a) Example from August 20, 2004 at 1605:56 UT. (b) Example from November 3, 2005 at 0344:29 UT.
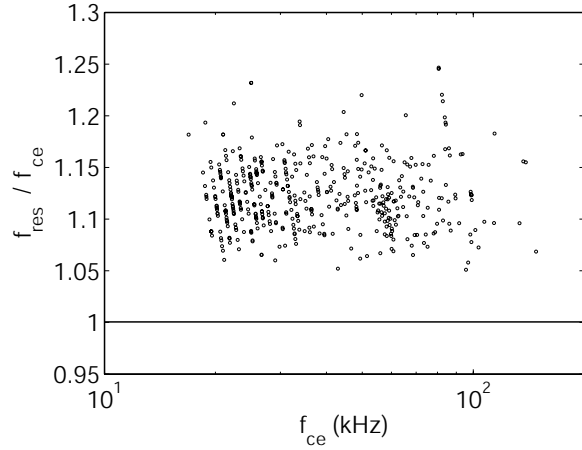
Figure 10. Plot versus log f_{ce} of f_{res}/f_{ce}, the ratio of the f_{ce}^+ resonance frequency to f_{ce} for observations in a four-month period May-August 2004.
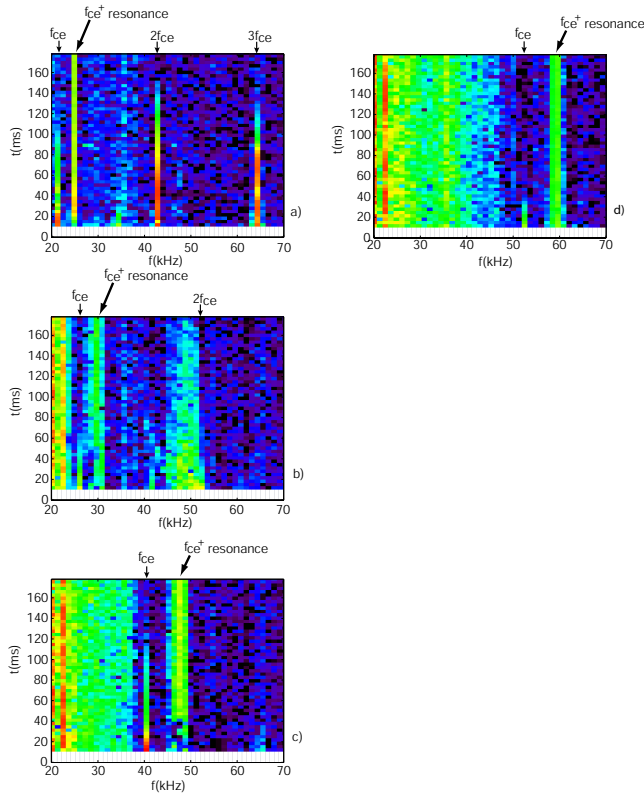
Figure 11. (a)–(d) Plasmagrams from an orbit on May 7, 2004 illustrating the appearance of f_{ce}^+ resonances in the frequency interval 20 - 70 kHz during soundings at decreasing altitude. The soundings were limited to 1200-Hz frequency steps instead of the 300-Hz resolution provided in Figures 2 and 6. The soundings began at 1656:24UT, 1701:24UT, 1711:24UT, and 1716:24UT, respectively.
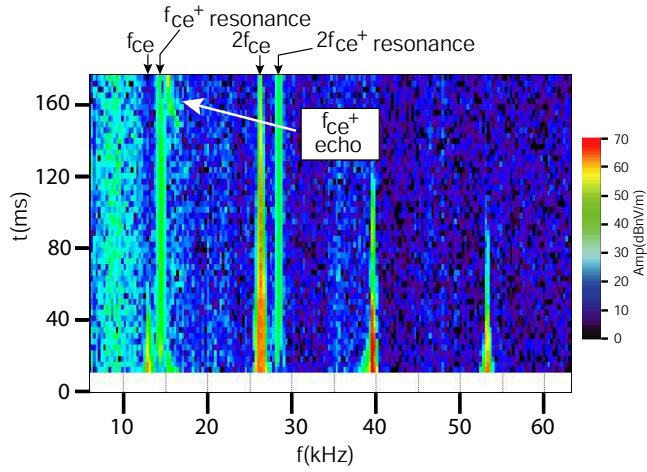
Figure 12. Plasmagram illustrating the occurrence of both an f_{ce}^+ resonance and a $2f_{ce}^+$ resonance. Both are weakly defined until ≈ 20 ms after the leading edge of the sounder pulse. A long range f_{ce}^+ echo also appears on this record from August 17, 2004 at 1636:58 UT.
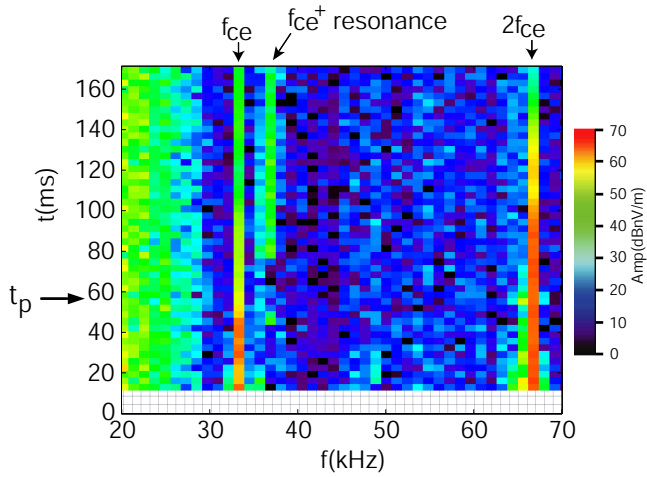
Figure 13. Plasmagram illustrating the apparent weakening of an f_{ce}^+ resonance at a time corresponding to the local proton gyroperiod t_p. The sounding began on July 29, 2004 at 1738:37.
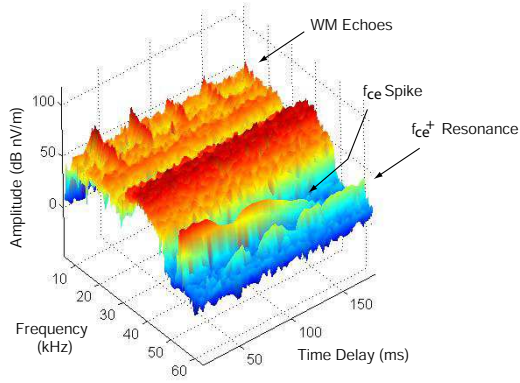
Figure 14. Three-D amplitude plot showing weakening of an $f_{ce}{}^+$ resonance at time delays corresponding to multiples of the local proton period as reflected in a series of echoes in the whistler mode domain. This is an expanded version of the event in Figure 16a below.
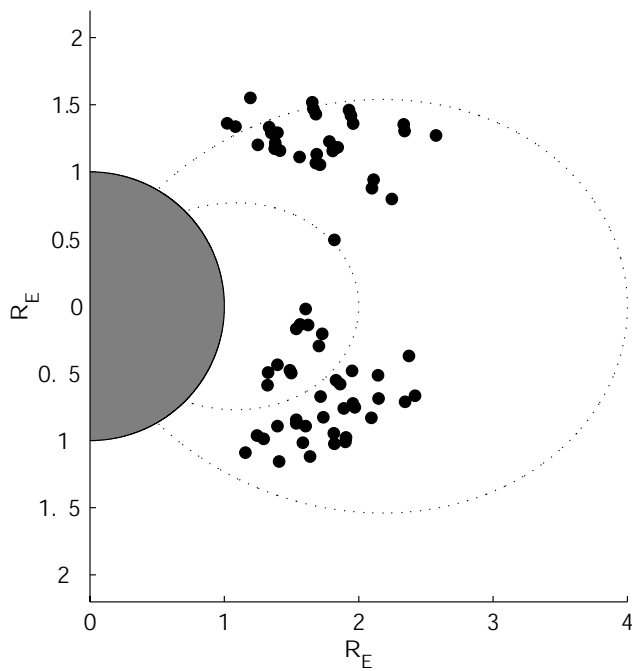
Figure 15. Meridian cross section of the magnetosphere showing locations where WM (whistler-mode domain) echoes were observed during two periods, November 1-20, 2001 and August 14-22, 2004. The locations in 2001 were all in the southern hemisphere, those from 2001 in the northern hemisphere.
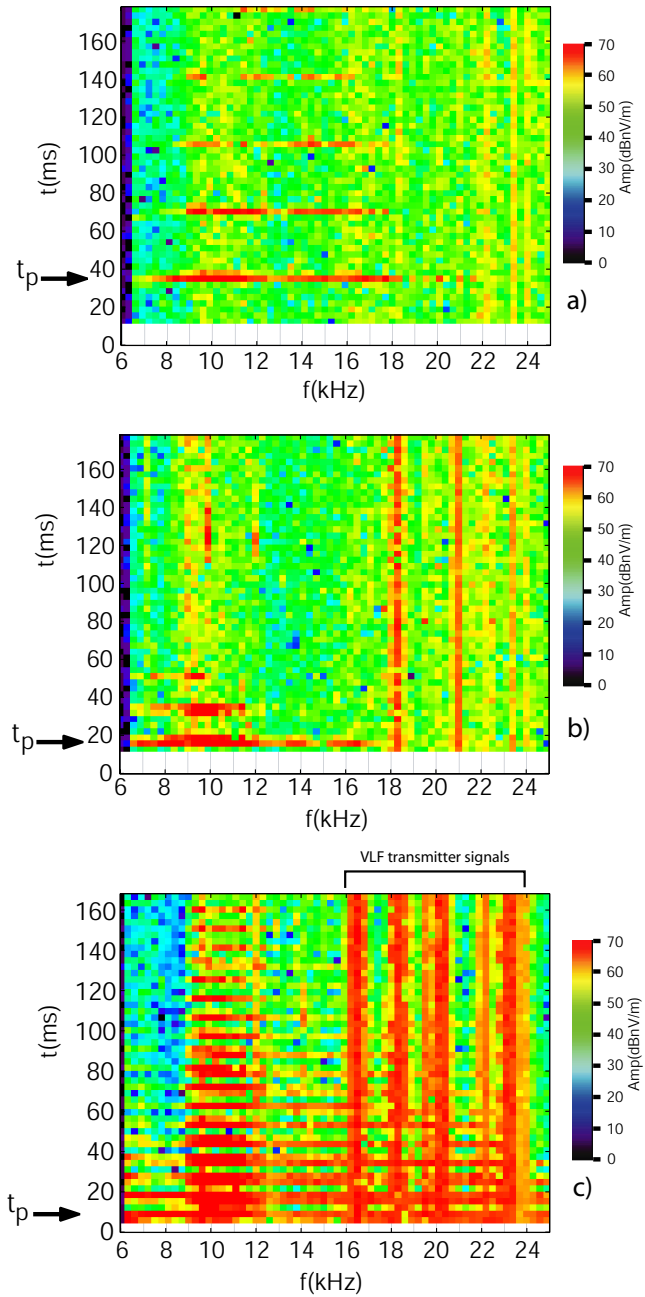
Figure 16. Portions of RPI plasmagrams showing examples of WM echoes recorded at various altitudes on three different IMAGE orbits. In each case, higher-order echoes appeared at multiples of the proton gyroperiod t_p. (a) Example from August 17, 2004 at 1712:38UT (also shown in Figure 14). (b) Example from August 20, 2004 at 1634:39UT. (c) Example from October 1, 2005 at 1141:07 UT. Echoes up to 18th order were detected. The vertical lines between 16 and 24 kHz represent whistler-mode transmissions from ground transmitters in Europe and part of Asia.
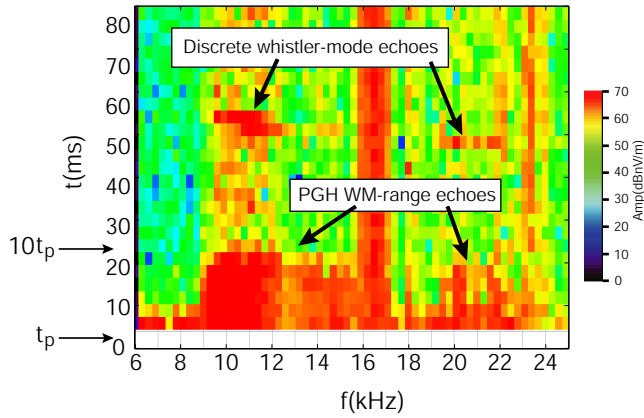
Figure 17. Portion of RPI plasmagram showing an example of WM echoes recorded on October 1, 2005 at an altitude of 1750 km. Since the local proton gyroperiod t_p was substantially less than the 6.4-ms separation between alternate RPI sampling intervals, the successive higher-order returns were merged on the record. The discrete whistler-mode echoes with delays near 55 ms are interpreted as having reflected from the bottom side of the ionosphere below IMAGE. This sounding followed the one of Figure 16c by $\approx$ 13 min.
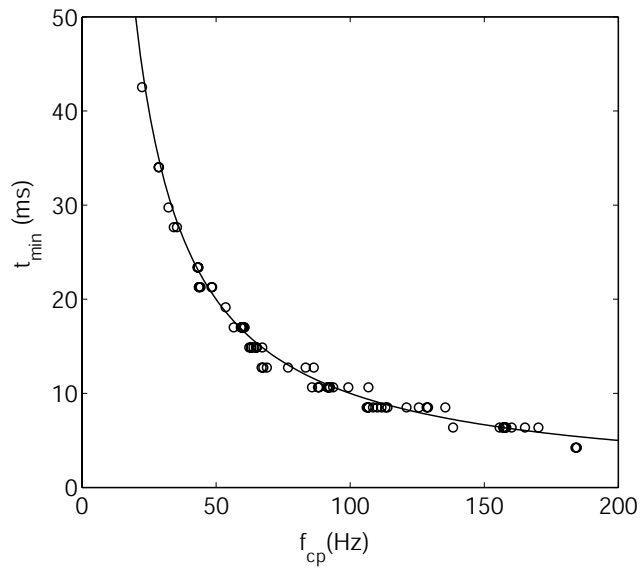
Figure 18. Plot of the delay time t_{min} of the initial or lowest-delay WM echo versus the local proton gyrofrequency f_{cp}. As in Figure 8, the solid curve represents the simple inverse relationship between the proton gyroperiod t_p and f_{cp}.
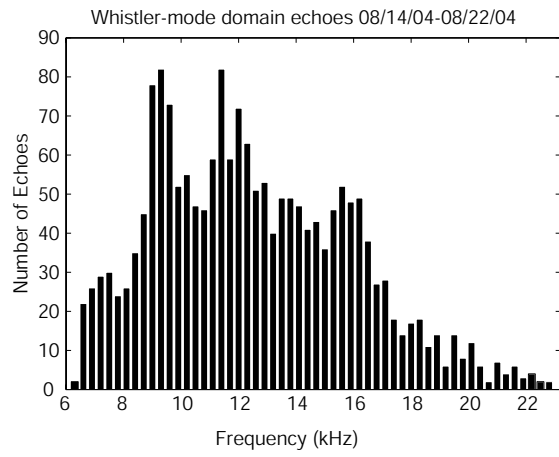
Figure 19. Histogram of the number of WM echoes at each frequency between 6 and 20 kHz during the two special observation periods November 1–20, 2001 and August 14–22, 2004. Echoes of all order were included.
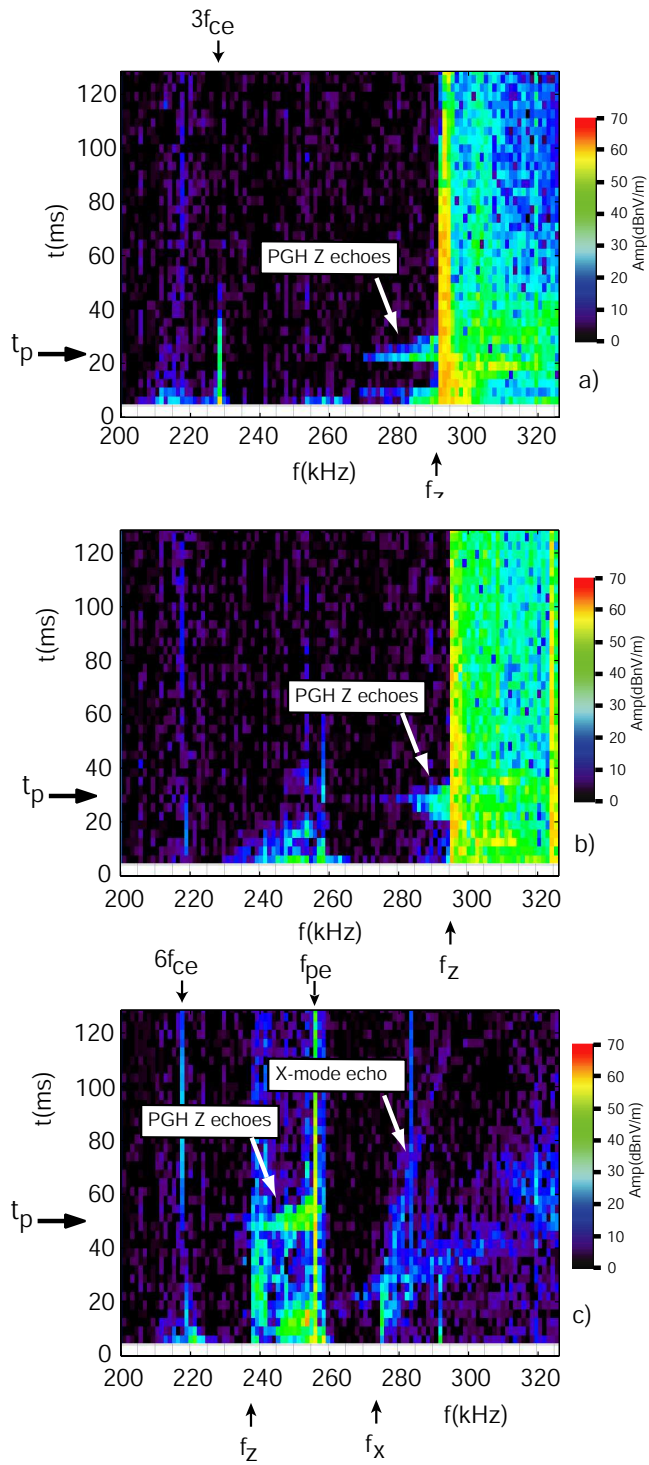
Figure 20. (a)–(c) Plasmagram examples of PGH *Z* echoes detected on three soundings during an outbound pass on August 14, 2005. The soundings began at 1150:48UT, 1153:49, and 1208:48, respectively. In Figure 20c a faint X-mode trace extends downward from long ranges to a cutoff at ≈ 273 kHz. There is also faint indication of an O-mode trace, as well as noise associated with Z-mode propagation.
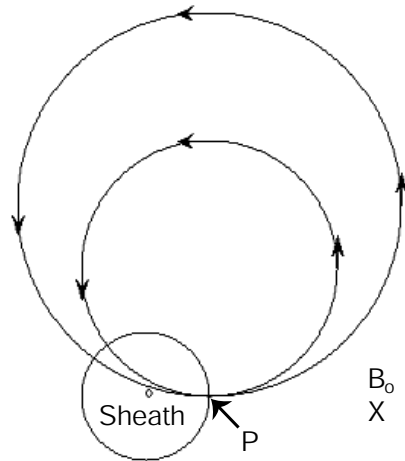
Figure 21. Schematic illustration of the WM echo mechanism. At the onset of an rf pulse, an electron sheath with a radius of ≈ 1 m forms around the positive-voltage antenna element. By virtue of their different original locations, protons within the sheath are energized by different amounts. Two are shown leaving the sheath at point P along the circumference of the sheath and then following circular trajectories that extend as much as several hundred meters into the neutral plasma outside the sheath. After one gyroperiod, the protons return to locations near the antenna where they take collective part in inducing a relatively large voltage on the antenna.